NACA RM L56A05

NACA

RESEARCH MEMORANDUM

USE OF SHADOWGRAPH TECHNIQUE IN THE ANALYSIS OF THE PERFORMANCE OF TWO SUPERSONIC AXIAL-FLOW COMPRESSOR ROTORS OPERATING OVER A MEAN RADIUS RELATIVE INLET MACH NUMBER RANGE OF 0.85 TO 1.7

By Theodore J. Goldberg and James R. Sterrett

Langley Aeronautical Laboratory
Langley Field, Va.

NATIONAL ADVISORY COMMITTEE FOR AERONAUTICS

WASHINGTON

April 4, 1956
Declassified October 14, 1957

NATIONAL ADVISORY COMMITTEE FOR AERONAUTICS

RESEARCH MEMORANDUM

USE OF SHADOWGRAPH TECHNIQUE IN THE ANALYSIS OF THE PERFORMANCE OF TWO SUPERSONIC AXIAL-FLOW COMPRESSOR ROTORS OPERATING OVER A MEAN RADIUS RELATIVE INLET MACH NUMBER RANGE OF 0.85 TO 1.7

By Theodore J. Goldberg and James R. Sterrett

SUMMARY

Shadowgraphs of the flow patterns through the blade passage and ahead of a compressor rotor were obtained by shining parallel light rays approximately radially onto the rotor hub and upstream inner ring which were painted white to serve as a screen. The visible flow patterns were used in conjunction with measured data to analyze the performance of two axial-flow supersonic compressors operating over a mean radius relative inlet Mach number range of 0.85 to 1.7 in Freon-12. This simple shadowgraph technique allowed a qualitative study of the starting mechanism, shock position and movement, and separation associated with shock boundary-layer interaction. This preliminary investigation shows the usefulness of the shadowgraph method in compressor analysis and demonstrates that further improvement in technique is warranted in order to obtain even more flow details.

A comparison with results from previous tests made with these two rotors in another test facility indicates the possibility of test-stand and tip-clearance effects on rotor performance.

INTRODUCTION

One of the most serious obstacles to the improvement of the supersonic compressor is the inability to obtain an actual knowledge of the internal aerodynamics. Previous analyses of the flow within supersonic compressors have been based upon the measured absolute inlet and exit flow parameters. The internal flow deduced in this way is very

unsatisfactory since the same absolute conditions can be obtained with many different blade shapes.

Studies of supersonic flow basically similar to that through compressor blading have been investigated in stationary experiments; for example, supersonic turning passages in references 1 and 2, supersonic diffusers in references 3 and 4, and shock boundary-layer interaction in references 5 and 6. However, the three-dimensional effects present in the compressor do not allow a direct application of the stationary results. In addition, to date there has been no way to verify the starting phenomenon hypothesized in references 7 and 8. A supersonic compressor was assumed to be started only when the weight flow remained constant with increasing back pressure.

The purpose of this paper is twofold: (1) to present a shadowgraph technique of obtaining the flow patterns through an axial-flow compressor rotor, and (2) to determine whether the flow pictures could be used in analyzing the operation of a supersonic compressor over the transonic and supersonic speed range. In particular, a visible flow pattern may allow a direct study of the shock locations, shock movements, and separation associated with shock boundary-layer interaction; it may verify the theoretical starting phenomena, and, in addition, it may augment the value of cascade tests by allowing a comparison of the flow patterns and establishing the range of operation within which correlation between rotor and cascade can be made.

The shadowgraphs were obtained by shining parallel light rays approximately radially onto the rotor hub, which was painted white to serve as a screen. Two supersonic compressors of the shock-in-rotor type, previously investigated in a different test facility and reported in references 9 and 10, were used in this preliminary investigation to determine the merit of this type of analysis. These rotors were chosen because of their peculiar weight-flow characteristic curves at high speeds since it was felt that the shadowgraphs might explain this phenomenon. Tests were made in Freon-12 without the design guide vanes over a mean radius relative inlet Mach number range of 0.85 to 1.7.

Because of the many variables involved and because no previous similar results were available, this investigation has been directed primarily toward a general understanding of the flow phenomena within the blade passages of a supersonic compressor.

SYMBOLS

a	velocity of sound, fps
C_p	specific heat at constant pressure, $ft^2/sec^2/^oR$

g	acceleration due to gravity (32.2 ft/sec^2)
M	Mach number, ratio of flow velocity to the velocity of sound, V/a
n	rotational speed of rotor, rps
P	total or stagnation pressure, lb/sq ft
p	static pressure, lb/sq ft
Q	torque, ft-lb
r	radial position measured from axis of rotation, ft
T	total or stagnation temperature, $^{\circ}R$
$\Delta T'$	isentropic stagnation-temperature rise, $^{\circ}R$, $T_o\left[\left(\frac{P_2}{P_o}\right)^{\frac{\gamma-1}{\gamma}} - 1\right]$
U	rotational velocity of blade element, $2\pi rn$, fps
V	velocity of fluid, fps
W	weight flow, lb/sec
x	distance in a plane perpendicular to the light rays
β	angle between axial direction and flow direction, deg
γ	ratio of specific heats
δ	ratio of actual inlet total pressure to standard sea-level pressure, $\frac{P_o}{2116}$
η_Q	torque efficiency, $\frac{C_p \Delta T' W}{2\pi n Q g}$
θ	ratio of actual inlet stagnation temperature to standard sea-level temperature, $\frac{T_o}{518.6}$
$W\frac{\sqrt{\theta}}{\delta}$	equivalent weight flow, lb/sec

$\frac{U_t}{\sqrt{\theta}}$ equivalent tip speed, fps

Subscripts:

t tip

o settling chamber

1 rotor entrance, stationary coordinates

1R rotor entrance, rotor coordinates

2 rotor exit, stationary coordinates

APPARATUS AND METHODS

Test Apparatus

Test stand.- A schematic drawing of the compressor test stand is presented in figure 1. Uniform, low-turbulence flow through a calibrated radial inlet is ensured through the use of three 60-mesh screens in conjunction with an area reduction of about 30 to 1 from the settling chamber to the straight entrance annulus. Downstream of the rotor the fluid is diffused by an annular diffuser having a constant outer wall diameter and incorporating straightening vanes. The exit pressure is controlled by a drum-type throttle valve incorporating a butterfly vane at the downstream face to reduce the pressure drop across the throttle. The throttle consists of two concentric perforated cylinders, the inner stationary and the outer rotated by an electric actuator. The butterfly valve is geared to the outer cylinder so that it is fully closed when the concentric holes are about half closed producing very sensitive throttle control. Two aircraft-type, water-cooled radiators are used to remove the heat of compression from the circulating fluid.

The rotor was driven through a 5.8 gear-ratio speed increaser by a 250-hp motor adapted for a reaction-type torquemeter incorporating a pneumatic pressure-cell measuring device.

A transparent plastic observation window was mounted in a 4- by 2-inch opening cut in the outer casing over the rotor and extended about 2 inches upstream of the rotor leading edge. A photograph of the observation window in the outer casing and the camera position is presented in figure 2. A flat and a curved constant-thickness window, the latter matching the contour of the casing, were used interchangeably without any noticeable difference in results.

Rotors.- Two 16-inch tip-diameter rotors having a hub-tip—radius ratio of 0.75 were used for this investigation and are described in references 9 and 10. The blades for both rotors are identical except one set has sharp leading edges while the other has a leading-edge radius of 0.010 inch. A photograph of the rotors is shown in figure 3. During the initial tests the tips of the blades having rounded leading edges were damaged and thus all tests reported herein were run with an average tip clearance of 0.073 inch as compared with 0.025 inch for the sharp leading-edge rotor.

Shadowgraph equipment.- The various components of the shadowgraph apparatus are shown in figure 4. In order to observe the flow through the blade passages, the motion of the rotor was stopped by a stroboscopic spark having a time duration of approximately one microsecond. The spark was triggered by an amplified input signal from an electromagnetic "pick-up" which was actuated by the rotation of the rotor shaft. The switch for the input signal of the amplifying circuit and the camera shutter were manually operated.

A 35-millimeter single-lens reflex camera with an f2.8 lens was used. The camera location can be seen in figures 2 and 4.

Most of the testing was done using a film with a daylight exposure index of 100. Near the completion of the program a better picture was obtained by using a film having a daylight exposure index of 200. However, when low light intensity is used for a subject having low contrast, the film should not be chosen solely on the basis of its exposure index, but on the basis of the largest density gradient and lowest density value for the toe of the film characteristic curve (density plotted against exposure). The film was developed for 6 minutes using Vividol developer mixed one part developer to one part water.

Instrumentation

Four static-pressure orifices spaced 90° apart in the settling chamber were used to measure the inlet total pressure. The inlet static pressure was measured 1 inch ahead of the rotor by four orifices spaced 90° apart on the outer and inner walls of the inlet annulus. A linear variation between the averages of the inner- and outer-wall static pressures was assumed. The upstream stagnation temperature was determined from a shielded total-temperature thermocouple rake located $3\frac{1}{2}$ inches ahead of the rotor.

Stagnation pressures and temperatures behind the rotor were determined from shielded total-pressure and total-temperature rakes located

approximately $\frac{3}{4}$ inch behind the trailing edge of the rotor hub. These rakes are shown in reference 10.

All temperatures were indicated on a commercial-type self-balancing potentiometer. All pressures were measured by a multiple-tube mercury manometer board and were recorded simultaneously by photographing the manometer. Automatic control valves were used to maintain constant preset values of settling-chamber pressure and temperature during test runs by controlling the rate of flow of supply Freon-12 and cooling water. The rotor speed was measured by a commercial stroboscopic tuning-fork-controlled instrument.

The velocity of sound in the Freon-12 air mixture was measured by an instrument similar to the one described in reference 11. From this measurement the proportions of the gas constituents and the physical characteristics of the mixture were determined.

Testing Procedure

In general, the procedure followed in operating the compressor consisted of obtaining the desired rotational speed at open throttle (minimum back pressure) and then taking data at various throttle settings up to the maximum throttle (maximum back pressure before audible surge) to determine the overall rotor characteristic curves. Using the shadowgraph apparatus previously described, photographs of the flow conditions upstream of and within the rotor were then taken for most throttle settings. At least two runs were made at each speed to check the repeatability of the data and flow patterns.

As a result of oil deposits on the window it was necessary to clean the window after only four or five throttle settings for each speed. The attraction of Freon-12 for oil in minute droplet form makes it difficult to eliminate these oil deposits in a system having any oil leakage.

Tests of the rotors were made without guide vanes over a range of equivalent tip speed from 444 to 840 feet per second in Freon-12. The settling-chamber pressure was maintained as high as the electrical rating of the drive motor would permit since better shadowgraphs are obtained with a higher density. Pressures varied from 0.3 atmosphere for high compressor work input to 0.8 atmosphere for low compressor work input. The Freon-12 purity varied from 95 to 99 percent by volume. The values of the gas properties corresponding to the purity measured for each test were used in the performance calculations.

Reduction of Data

The inlet Mach numbers were based upon inlet wall static and settling-chamber pressure measurements. The rotor operating characteristics were determined in the following manner:

1. The total-pressure ratio across the rotor was determined from the ratio of the arithmetical average of the downstream total pressure to the upstream total pressure which was assumed to be equal to the settling-chamber pressure. The pressure ratios given for the shadowgraphs were obtained from a gage which was connected to a downstream total-pressure rake and the settling chamber and therefore may not be identical to the arithmetically averaged values.

2. The weight flow was measured by a calibrated inlet.

3. Two methods were used to determine the rotor efficiency, one based upon measured total-temperature rise and the other based upon measured torque. For the sharp leading-edge rotor these two efficiencies agreed on the average within ±2 percent with an occasional maximum difference of 6 percent. However, for the rounded leading-edge rotor the temperature-rise efficiency was consistently from 8 to 16 percent lower than that obtained from the torque measurements. All values of efficiency presented are those based upon torque measurements.

SHADOWGRAPH INTERPRETATION

Theory

Discussions of the shadowgraph method have been given in many publications (for example, refs. 12 and 13). Some of the important characteristics that are useful in the interpretation of shadowgraph photographs are repeated herein for the clarity of this paper.

When light passes through a gas having density variations perpendicular to the rays, the light rays are diverted from their original directions. In a region where the density change is constant, the deflection of the rays is constant and no change in the light intensity will result at the screen. In a region where the density change is not constant, a change in the light intensity will result at the screen. In short, the shadowgraph indicates only the second derivative of density with respect to distance normal to the light beam. Therefore, a

shadowgraph is capable only of showing the edges of a shock where $\frac{\partial^2 \rho}{\partial x^2} \neq 0$ but not an expansion region where $\frac{\partial^2 \rho}{\partial x^2} \approx 0$.

The deviation of the light rays is proportional to the path length of the rays through the density gradient. Therefore, the path length as well as the magnitude of $\frac{\partial^2 \rho}{\partial x^2}$ affects the contrast of the shadow on the screen.

The longer the optical lever arm (the distance from the disturbance to the screen), the greater is the sensitivity of the system up to a limiting value. If the screen is located at the density gradient, the shadowgraph effect practically disappers.

Hypothesis

In three-dimensional flow, the interpretation of a shadowgraph may become complicated. For example, a shadowgraph of a sphere in a supersonic wind tunnel would show only the beginning of the shock envelope and its intersection with the walls (perpendicular to the light) where $\frac{\partial^2 \rho}{\partial x^2} \neq 0$ but not the rest of the envelope for which $\frac{\partial^2 \rho}{\partial x^2} \approx 0$. Similarly, in the present application where parallel light perpendicular to the axis of rotation is shining radially onto the hub of a rotor, the resulting shadowgraph would be expected to indicate the boundaries of the shock envelope which would be at the tip and root, and any boundaries in between where the light rays are tangential to the shock or where there are sudden radial changes in the shock.

When interpreting the shadowgraphs taken in the present investigation, it seems reasonable to assume the following:

1. At the leading edge of the blade the tip section always produces supersonic velocities relative to the blade before the root section; thus any existing shock will always start at the tip of the blade and extend down part way, or all the way, to the root depending upon the rotational speed. Therefore, one visible shock in the shadowgraph is the boundary of the shock envelope which exists at a section near the tip because of the large optical lever arm. Another shock which may be visible is the boundary where the light is tangent to the shock envelope. This point of tangency must occur below the tip but it will not produce a shadow if it occurs very near the root where a density change is not visible due to the absence of a sufficiently long optical lever arm. A sketch

showing the expected types of shock envelope is presented in figure 5. Because of the blade geometry of these rotors, it is very unlikely that there are any sudden changes of the shock in the radial direction and, therefore, no more than two visible shocks are expected from one shock envelope.

2. Reasoning similar to the above can be applied to all shocks within the blade passage. However, if a separated flow region exists near the tip, the strength of any shock entering this region would gradually decrease. Density changes perpendicular to the light rays would thus be very gradual $\left(\frac{\partial^2 \rho}{\partial x^2} \approx 0\right)$ and the tip shock boundary may not be visible. Thus, because of separation and the orientation of the shocks with the light rays, the tip shock boundary may not always be visible and the radial location of shocks within the blade passage other than the leading-edge shock may become difficult to determine.

3. Since the orientation of the light rays with the shock varies with blade position and shock position, the shock strength cannot be determined from the shadowgraph. In fact, the shocks may not always be visible in all passages.

Orientation

As an aid to interpreting these shadowgraphs, photographs of the stationary rotor in the testing position are presented in figure 6. Both photographs were taken with parallel light shining radially onto the hub and with the camera located in the same position as used for the shadowgraphs. The three-dimensional effect can be seen in figure 6(a) when continuous light is used to provide sufficient illumination on all parts of the blade. However, with lower illumination from a single flash with the spark source used to obtain the shadowgraphs, the three-dimensional effect disappears and only a silhouette of the blade remains as shown on figure 6(b). Because of the twist in the blade the shadow cast on the hub is a projection not of any one section but of the composite blade. Inasmuch as the leading edge is a radial line, it projects as a point when the leading edge of the blade is alined with the parallel light, but because the trailing edge is not a radial line, its tip is projected as a "V-shaped" shadow. The diagonal lines in a chordwise direction are the joints between the blade base and the rotor hub.

RESULTS AND DISCUSSION

The figures presenting the test results for the two rotors are tabulated below:

Type of data	Rotor	
	Sharp leading edge	Rounded leading edge
	Figure	
Shadowgraphs near open throttle	7	8
Shadowgraphs for varying throttle	11	15
Rotor characteristic curves	13	14
Relative inlet Mach numbers	12	16
Relative inlet angles	10	17

Starting Phenomenon

For supersonic compressor rotors designed with a convergent-divergent blade passage, a problem exists in regard to the starting of supersonic flow. When the leading-edge shock is oblique, supersonic flow must exist within the passage ahead of the minimum and the passage must be started. However, a started supersonic flow may also exist even though the leading-edge shock is not completely oblique because of the blade geometry. Therefore, a started condition can be defined to exist when, for a fixed Mach number, the wave pattern at the leading edge of the blade is a function only of the blade geometry and is completely independent of conditions at the minimum section.

An examination of figure 7 shows that, as the rotational speed of the rotor (and consequently the relative velocity entering the blades) increases, the upstream bow waves move closer to the blade leading edge and the normal shock ahead of the passage gradually moves into the passage and becomes oblique. At the speed where the leading-edge shock moves into the passage and becomes oblique, the passage is started. These photographs show that the starting process occurs gradually with no apparent discontinuity in the performance of the compressor. This is in agreement with the Kantrowitz hypothesis given in reference 7.

The two leading-edge shocks which appear in figures 7(c) through 7(f) (best picture 7(f)) must come from a shock envelope similar to the one shown in figure 5(a). In figures 7(e) and 7(f) the shock closest to the leading edge appears to be oblique indicating a started condition

near the tip while the shock furthest from the leading edge, which comes from some section below the tip, appears to be normal indicating a choked condition from that radius down to the root. Both leading-edge shocks become forked at the suction surface as a result of an inability to reflect from the suction surface or to shock boundary-layer interaction; it is this "forking" which makes the oblique shock appear normal near the suction surface. The complete blade passage can be seen to be started in figure 7(g) because the leading-edge shock must be oblique in order to reflect off the suction surface. In figures 7(g) to 7(l) the leading-edge shock is seen to move further into the passage and appears to become attached in figure 7(i).

In general, the shadowgraphs of figure 8 show that the starting process for the rounded leading-edge blades is similar to that for the sharp leading-edge rotor. While there is a possibility that the passage may be started in figure 8(e), it appears to be definitely started at 655 feet per second (figure 8(f)), which is approximately the same tip speed at which the sharp leading-edge rotor started.

The maximum contraction ratio, the ratio of the entrance area to the minimum area, which permits starting of supersonic flow for a given entrance Mach number has been presented in reference 3. The one-dimensional starting Mach number for these blades in Freon-12 gas as a function of radius r is shown as a dot-dashed curve in figure 9 along with the measured variation of relative inlet Mach number for various tip speeds. From this figure it appears that the passage would not be expected to start for tip speeds below 630 feet per second. However, expansion waves about the leading edge will increase the relative inlet Mach numbers for the portion of the blade operating at relative inlet angles (shown in fig. 10) greater than the blade setting angle of 60°. This increased Mach number, shown in figure 9 as dashed curves, may explain the starting of a portion of the passage at tip speeds below 630 feet per second. In addition, the presence of a detached shock and the effect of local separation about the leading edge may allow starting before the theoretical starting Mach number is reached as discussed by Ferri in reference 8. From this preliminary investigation it is not known whether the starting of the passage is gradual, continuing progressively from tip to root, or if after a small portion near the tip becomes started, the rest of the passage starts at the same time.

Flow Phenomena for Sharp Leading-Edge Rotor

Leading-edge effects at minimum back pressure.- A further study of the shocks about the leading edge of the blade reveals additional information about the flow phenomena which cannot be determined from the usual temperature, pressure, and angle measurements. Although it does not show

up clearly in all pictures, there is a shock in figures 7(c) to 7(h) (best picture 7(g)) which comes from the suction surface near the leading edge. This shock is probably caused by local flow separation and overexpansion about the leading edge and its presence indicates that the leading-edge shock must be detached at the radius at which the "overexpansion shock" occurs. The radial location of this shock cannot be determined from the shadowgraph since it can occur with the blade at either positive or negative angles of attack as seen in unpublished interferograms. However, it is apparently at the same radial station as the shock furthest from the leading edge of the blade since they coalesce at a point ahead of the rotor as seen in figures 7(c) to 7(f) (best picture 7(e)). For speeds above 695 feet per second the "overexpansion shock" can no longer be seen and the leading-edge shock appears to become attached.

At the speeds where the leading-edge shock was considered to be attached (figs. 7(i) to 7(l)) an attempt was made to compare the leading-edge shock angles in the shadowgraphs with those computed from the tip leading-edge wedge angle and the tip relative inlet Mach numbers after expansion waves due to angle of attack. The measured shock angles for these speeds were on the average about 6° greater than the calculated angles, which in terms of Mach number would mean a difference of about 0.2. This difference may be due to the inaccuracy of measurements made from the shadowgraphs, the presence of optical distortions in the shadowgraphs, and the inability to determine accurately the relative inlet Mach number due to the varying flow field upstream of the rotor.

Rearward-shock effects with increasing speed.- An examination of figure 7(a) shows a normal shock in the passage. As the rotational speed of the rotor is increased the normal shock moves further downstream and eventually becomes oblique as can be seen in figure 7(e). If the visible boundary of the rearward shock were from the tip section in figures 7(e) through 7(l), it would have to originate downstream of the tip trailing edge. However, it is very unlikely that a shock originating behind the blade passage in a constant annular area could maintain a stable condition. Therefore, this visible shock boundary of the rearward shock apparently moves toward the hub as it moves downstream with increasing rotor speed. The existence of separation along the outer casing, which increases toward the rotor trailing edge due to centrifugation of the boundary layer and separated flow from the blade surfaces in addition to the boundary-layer buildup along the casing, would explain why the shock boundary at the tip is not visible; this reason was previously discussed in the assumptions under "Shadowgraph Interpretation." The determination of the radial location of the visible shock boundary is further complicated due to the inevitable forking of the shock as it extends up into the separated region.

From the shape of the normal shock in figure 7(a) there is no indication of separation; however, as the normal shock moves back in the

passage, it becomes increasingly forked indicating flow separation along the suction surface due to shock boundary-layer interaction. At the higher speeds, separation is also indicated along the pressure surface by the fact that the stem of the rearward shock becomes forked at the pressure surface of the blade; for example, in figures 7(j) through 7(l) the rearward shock appears as an "X" instead of a "Y" as for lower speeds. Although the degree of separation downstream of the shock cannot be determined from the shadowgraphs, an examination of the legs of the fork shows that on the suction surface the starting point of separation (herein defined as the point at which the upstream leg of the fork intersects the suction surface) moves downstream as the rotational speed is increased. An example of this can be seen by comparing figures 7(d) and 7(g). In figure 7(d) the downstream leg of the fork does not extend to the blade outline indicating a region of separation; in figure 7(g) the upstream leg of the fork, which is now at the same chordwise position as the downstream leg of the fork in figure 7(d), extends up to the blade outline indicating little, if any, separation now present at this point. In addition, because there is little separation ahead of the upstream leg of the shock, the flow ahead of the normal shock has reattached if separation resulted from the interaction of the leading-edge shock with the boundary layer.

Effects due to increasing back pressure.- Shadowgraphs of the flow at various speeds and throttle settings are presented in figure 11. The extraneous patterns visible in many of these pictures result from oil deposited on the observation window during the course of a run. This oil is readily discernible, sometimes as smears over a large region as seen in figure 11(a) for maximum back pressure, but more often as dark, nearly vertical streaks as in figure 11(c).

In figure 11(a) it can be seen that with increasing back pressure the normal shock in the passage is pushed upstream through the throat whereupon it coalesces with the entrance normal shock. As this shock moves forward, the upstream leg of the fork gets shorter and disappears indicating a disappearance of the separation associated with shock boundary-layer interaction on the suction surface. The leading-edge shocks are also moved forward with increasing throttle indicating a decrease in relative inlet Mach number and an increase in relative inlet angle, and hence a decrease in weight flow. The changes in these parameters are verified by the measured values shown in figures 12, 10, and 13(a).

The shocks at the rear of the passages in figures 11(b) through 11(e) are pushed forward and become normal with increasing back pressure. However, the normal shocks are not moved up to the throat; this prevents the attainment of the theoretical maximum diffusion and pressure recovery and therefore results in poor efficiencies as seen in figure 13(b). Although the normal shock is not pushed to the minimum area of the passage, the shocks from the leading edge can be seen to be affected by back pressure.

In figures 11(b) and 11(c) the leading-edge shock becomes almost normal at maximum pressure ratio while in figures 11(d) and 11(e) only the reflections from the leading-edge shocks are obviously affected by back pressure. However, inasmuch as the weight flow decreases with increased back pressure, as seen in figure 13(a), the leading-edge shock must also move slightly in figures 11(d) and 11(e). Since the Mach number at the throat is equal to, or greater than, 1.0 at all radial stations, any disturbance affecting the leading-edge shock can only be transmitted through the boundary layer or separation existing on the blade surface and/or the outer casing. This fact is supported by the forward movement of the oil streaks with increasing throttle as seen in figures 11(b) and 11(c) which is apparently caused by the propagation of pressure disturbances through the separation along the outer casing. In figure 11(f) there is no apparent effect on the leading-edge shock or its reflection due to throttling. This is substantiated by the vertical weight-flow characteristic curve in figure 13(a).

Previous analyses of rotor characteristic curves could not resolve the question of whether a supersonic compressor was started if the weight flow decreased with increasing back pressure. In figure 13(a) at 695 and 730 feet per second the weight flow decreases with increasing back pressure but it can be seen in figures 11(d) and 11(e) that the passage remains started at maximum throttle. This proves that a decrease in weight flow does not necessarily indicate an unstarted condition.

Flow Phenomena for Rounded Leading-Edge Rotor

Leading-edge effects at minimum back pressure.- In general, the shock patterns obtained for the rounded leading-edge blades for varying speeds near open throttle (fig. 8) are similar to those obtained for the sharp leading-edge rotor. The leading-edge shocks can be seen to remain detached at all speeds as would be expected because of the blunt leading edges. The shock from the suction surface caused by overexpansion appears at all speeds, whereas for the sharp leading-edge blades it could not be seen at the higher speeds. For speeds at which this overexpansion shock appears for both rotors, it does not extend as far from the suction surface of the rounded leading-edge rotor as it does for the sharp leading-edge rotor. This is consistent with the expectation of less separation and thus less overexpansion about a rounded leading-edge blade operating at about the same angle of attack as a sharp leading-edge blade. The appearance of the overexpansion shock at the higher speeds only for the rounded leading-edge rotor may be due to the larger angle of attack as can be seen from a comparison of figures 10 and 17.

At the lower speeds the strength of the upstream waves is unknown and a comparison of the shock slopes of the two rotors cannot be made.

However, the upstream waves can be considered to approach Mach waves in figures 7(h) through 7(l) and figures 8(g) through 8(j). the smaller Mach angle (measured from the relative inlet direction) produced by the rounded leading-edge blades indicates a smaller weight flow than that produced by the sharp leading-edge blades which is in agreement with the measured values presented in figures 13(a) and 14(a).

Effects due to increasing back pressure.- Only a few representative speeds showing the effect of back pressure on the rounded leading-edge rotor are presented in figure 15 to show the similarity of the shock patterns obtained for the two rotors. For all speeds the shock in the rear of the passage is moved forward only a relatively short distance and becomes normal. As in the case of the sharp leading-edge rotor this indicates poor diffusion and pressure recovery resulting in poor efficiency (fig. 14(b)). Over the entire speed range the leading-edge shock is markedly affected by back pressure. The forward movement of the leading-edge shock results in a decrease in the relative inlet Mach number, an increase in the relative inlet angle, and a decrease in weight flow. The changes in these parameters are confirmed in figures 16, 17, and 14(a), respectively. Unlike the performance of the sharp leading-edge rotor, a vertical weight-flow characteristic curve is never attained for the rounded leading-edge blades.

At and about design speed the greater effect of back pressure on the leading-edge shock for the rounded leading-edge blades indicates the presence of more separation on the suction surface than for the sharp leading-edge blades. The exact reason for this increased separation cannot be determined from these shadowgraphs but the increase may be caused by a variation of one or more of the following: increased tip clearance, increased shock strength at the suction surface, reduced distance from the leading edge to the point where the shock intersects the suction surface, and type of boundary layer along the suction surface due to leading-edge effects. This increased separation indicates a radical difference in the flow through the passages of the two rotors and is a predominant factor in accounting for the poorer performance of the rounded leading-edge blades.

Supplementary Applications to Compressors

Methods of obtaining additional information.- The use of the shadowgraph in rotor investigations at first appears limited to the interpretation of the tip shock boundaries and points of tangency on the shock envelope. However, a further study of the flow can be made by generating shocks from disturbances placed in the flow field.

A more exact radial location of the visible shocks may be determined by observing the coalescence or interaction of these visible shocks with superimposed generated shocks. It may also be possible to study the flow

at other radial stations from visible patterns induced by generating shocks at various radial positions. This method would give more details of the starting process insofar as determining whether starting occurs in gradual increments from tip to root or over the entire span at the same time. Regions of separation on the blade surfaces, besides those indicated by forked shocks, may be determined by placing scratches on the blade and noting where these scratches no longer generate shocks.

At the conclusion of the present investigation an attempt was made to superimpose shocks from scratches on the blade surface and bumps of plastic at the leading edges of the rounded leading-edge rotor. Shocks generated by the above methods were clearly visible; however, before any additional information about the flow field could be obtained, the rotor was badly damaged by pieces of plastic which were flung off the blades.

Enhancement of cascade application.- As in subsonic compressor investigations, it is convenient to study transonic and supersonic compressor blading in two-dimensional cascades. It is, of course, impossible in a stationary experiment to duplicate the three-dimensional flow in a rotor. In addition, the flow patterns of certain rotor designs, such as those requiring spillage, cannot be duplicated in two-dimensional cascades and, therefore, at present comparison with design theory can be made only from visible flow patterns obtained in three-dimensional cascades. However, since most rotor designs can be duplicated in a stationary cascade, the ability to obtain a visible flow pattern for transonic and supersonic rotors permits a comparison with the flow pattern obtained from two-dimensional cascades. A comparison of the flow pattern would help to determine the extent of the three-dimensional effects by furnishing an additional correlation factor and thus enhance the usefulness of the two-dimensional cascade as a tool for compressor research.

Unfortunately, two-dimensional cascade flow pictures for the tip section of the rotor design used in the present investigation are not available; consequently, correlation between the rotor and cascade cannot be made for the tip section. However, schlieren photographs of the flow through a stationary cascade having blades the same as the pitch section of the sharp leading-edge rotor are presented in figure 18. Inasmuch as the shadowgraphs obtained for the rotor operating near design speed were interpreted to have only one boundary for each shock envelope indicating no sudden radial changes of the flow in the rotor, it is reasonable to assume that the shock patterns at the pitch are similar to those at the tip. The cascade tests were made in air at a Mach number of 1.60.

In the cascade the passage did not start at the design Mach number of 1.55 in spite of the fact that the theoretical starting Mach number in air is 1.39. In the rotor, where the theoretical starting Mach number in Freon-12 is 1.34 for the pitch section, the complete blade passage can

be seen to be started in figure 7(g) at which speed the pitch Mach number was 1.33 assuming a straight-line variation from figure 12. The fact that the pitch section could not start in the cascade at a higher Mach number than the theoretical starting Mach number but did start in the rotor at about the theoretical starting Mach number shows that there must be large three-dimensional relieving effects in a rotor for this blade design which must be considered in correlating cascade with rotor data.

The cascade shock patterns for the open and partial throttle conditions are, in general, similar to those obtained with shadowgraphs of the rotor. At maximum throttle it is apparent that in the cascade there is a marked effect of back pressure on the leading-edge shock. This effect must be attributed to the separation on the suction surface which provides the only means through which any downstream disturbance can be propagated. This conclusion substantiates the analysis previously made from the examination of the shadowgraphs where the leading-edge shock was affected by back pressure when a normal shock existed in the passage. In contrast to the cascade operation at maximum back pressure, the shadowgraphs for the sharp leading-edge rotor operating at about the same inlet Mach number showed very little, if any, effect on the leading-edge shock due to back pressure. While the exact reason for this dissimilarity is not known, it shows different operating characteristics for the rotor and cascade. Although the operation of the blades tested in cascade obviously should not be compared with the rounded leading-edge rotor since the results of the two rotors are different, nevertheless, it is interesting to see that a similar leading-edge shock deformation is attained in both the rotor and cascade under conditions of maximum back pressure.

The ability to compare the shock patterns obtained from the rotor and cascade may be an important factor in explaining any differences in operation and in establishing the range of operation within which correlation between rotor and cascade can be made.

Corroboration of Shadowgraph Analysis

After completion of the present investigation and the above analysis, the sharp leading-edge rotor was used for a different test program. During the new investigation the upstream ring, which was fabricated from plastic, rubbed against the rotor producing a charred, black dust. These particles apparently fused with the paint on the blades and rotor hub forming a pattern as shown in figure 19. This pattern was noticed upon completion of a run at a speed slightly above design at a pressure ratio of approximately 1.7. Since it is not known exactly when, or for how long, the rubbing occurred, a direct comparison between the dust pattern and any one particular shadowgraph cannot be made. However, in general, these patterns are similar to the shock patterns deduced from the shadowgraphs.

The pattern at the center of the blade profile in figure 19(b), which is from the intersection of the leading-edge shock with the suction surface, can be seen to extend all the way to the tip with no sudden radial changes. Therefore, the shadowgraphs at about design speed would, and did, show only the tip leading-edge shock boundary. The rearward shock envelope can be seen to extend from the suction surface to the pressure surface from the shock pattern on the hub which occurs over the numbers printed on the hub (fig. 19(a)). On the suction surface the pattern from the rearward shock does not extend to the tip within the passage; on the pressure surface the rearward shock pattern becomes forked near the tip of the blade indicating the presence of separation on the outer casing. These shock configurations may explain why the rearward shock is not visible at the tip section in the shadowgraphs at the high speeds. In general, the dust patterns tend to substantiate the analysis made from the shadowgraph pictures.

The rearward shock patterns on both surfaces show a curvature which would produce a point of tangency with a radial line. From shadowgraph theory the shock boundary at this point should be visible provided there is a sufficiently long optical lever arm. Actually, in some of the shadowgraphs two rearward shocks are visible; for example, in figure 11(e) at $P_2/P_1 = 1.77$. In interpreting the shadowgraphs, it was not known whether the additional shock was due to instability or to a point of tangency. These dust patterns tend to indicate that the second rearward shock in the shadowgraphs is due to a point of tangency.

Previously, attempts were made to produce shock patterns within the blade passages of a supersonic rotor by means of injecting lampblack upstream of the lightly oiled rotor. Without shadowgraphs the interpretation of the resultant patterns, which were not as distinct as the present dust patterns, was not possible.

Comparison with Previous Results

The rotors used in this investigation were previously tested in a different compressor test stand, described in reference 10, and the results were reported in references 9 and 10. The operating characteristics for both rotors obtained in the present test facility, herein designated as test stand A, and the operating characteristics obtained in the previous test facility, herein designated as test stand B, are compared in figure 20. The agreement in the performance for the sharp leading-edge rotor (fig. 20(a)) in both test stands is within experimental accuracy up to a tip speed of 700 feet per second. However, above this speed at maximum throttle the pressure ratio, weight flow, and efficiency were higher in the present test stand and showed no peculiarities in the weight-flow characteristics as was observed in the other test

stand and reported in reference 9. It is assumed that painting the rotor had no effect on its performance since the maximum thickness of the paint was 0.002 inch. Therefore, since the rotor, test conditions, and instrumentation were the same for both investigations, the difference in performance at high speed and maximum throttle can only be attributed to test-stand effects. Some of the differences in the two test facilities are outlined below:

1. Inlet: test stand A - radial inflow
   test stand B - straight inflow

2. Inlet annulus: test stand A - straight for 6 inches ahead of rotor
   test stand B - straight for 1 inch ahead of rotor

3. Diffuser: test stand A - straight annular diffuser
   test stand B - radial diffuser

4. Volume: test stand A - 112 ft^3
   test stand B - 240 ft^3

A comparison of the results of the rounded leading-edge rotor in the two facilities (fig. 20(b)) shows a variation in performance over the entire speed range at maximum throttle. The performance in test stand A was better for speeds above 750 feet per second but poorer at lower speeds. There were no discontinuities or peculiar characteristic curves at the high speeds in test stand A that were obtained in test stand B and reported in reference 10. Since any test-stand effects would be expected to have a similar effect on both rotors, the greater difference in performance of the rounded leading-edge rotor which is obvious at speeds below 680 feet per second can apparently be attributed to tip clearance. Although it was not the purpose of this investigation to examine the effects of tip clearance, and this isolated case is by no means conclusive, it appears that tip clearance may be considered an important parameter in supersonic compressor tests.

CONCLUDING REMARKS

A method of obtaining the flow pattern through an axial-flow compressor rotor by means of shadowgraph and its application in analyzing the operation of two supersonic compressors operating in Freon-12 over a mean radius relative inlet Mach number range of 0.85 to 1.7 is presented. The following conclusions are drawn:

1. Visible shock patterns ahead of the rotor and within the blade passages can be obtained by the shadowgraph method.

2. A qualitative interpretation of the flow pattern, such as shock position, shock movement, and separation associated with shock boundary-layer interaction, can be made from the shadowgraphs.

3. The shadowgraphs show when a rotor starts and that the starting process occurs gradually with no apparent discontinuity in the performance of the compressor. In addition, the shadowgraphs show that a decrease in weight flow with increasing back pressure does not necessarily indicate an unstarted condition.

4. In general, the shadowgraph is most suited for obtaining the flow pattern at or near the tip section which makes it particularly applicable to transonic rotor investigations.

5. The exact radial location of all visible shocks can not be determined from the shadowgraphs alone. However, when used in conjunction with the usual measured data (pressure, temperature, and so forth), the shocks may be qualitatively located. It is believed that greater accuracy of the radial shock locations can be attained by observing the shock generated from a disturbance placed in the flow field at different radial positions. In addition, more flow details can be attained from improved techniques such as increased sensitivity and varying camera and light orientation.

6. The shadowgraph presents a means of comparing the flow patterns within rotors and cascade sections, thus enhancing the usefulness of cascade results.

7. This preliminary investigation shows the usefulness of the shadowgraph as a tool for compressor analysis and warrants further investigation.

8. The performance and operating characteristics at high pressure ratios of the rotors used in this investigation were not the same as the characteristics obtained from these rotors previously tested in another facility. This indicates the possibility of serious test-stand and tip-clearance effects on the performance of supersonic compressor rotors.

Langley Aeronautical Laboratory,
National Advisory Committee for Aeronautics,
Langley Field, Va., December 16, 1955.

REFERENCES

1. Boxer, Emanuel, Sterrett, James R., and Wlodarski, John: Application of Supersonic Vortex-Flow Theory to the Design of Supersonic Impulse Compressor- or Turbine-Blade Sections. NACA RM L52B06, 1952.

2. Liccini, Luke L.: Analytical and Experimental Investigation of 90° Supersonic Turning Passages Suitable for Supersonic Compressors or Turbines. NACA RM L9G07, 1949.

3. Kantrowitz, Arthur, and Donaldson, Coleman duP.: Preliminary Investigation of Supersonic Diffusers. NACA WR L-713, 1945. (Formerly NACA ACR L5D20.)

4. Erwin, John R., Wright, Linwood C., and Kantrowitz, Arthur: Investigation of an Experimental Supersonic Axial-Flow Compressor. NACA RM L6J01b, 1946.

5. Lange, Roy H.: Present Status of Information Relative to the Prediction of Shock-Induced Boundary-Layer Separation. NACA TN 3065, 1954.

6. Bogdonoff, S. M., and Kepler, C. E.: Separation of a Supersonic Turbulent Boundary Layer. Jour. Aero. Sci., vol. 22, no. 6, June 1955, pp. 414-424, 430.

7. Kantrowitz, Arthur: The Supersonic Axial-Flow Compressor. NACA Rep. 974, 1950. (Supersedes NACA ACR L6D02.)

8. Ferri, Antonio: Preliminary Analysis of Axial-Flow Compressors Having Supersonic Velocity at the Entrance of the Stator. NACA RM L9G06, 1949.

9. Goldberg, Theodore J.: Experimental Investigation of an Axial-Flow Supersonic Compressor Having Sharp Leading-Edge Blades With an 8-Percent Mean Thickness-Chord Ratio. NACA RM L54K16, 1955.

10. Goldberg, Theodore J., Boxer, Emanuel, and Bernot, Peter T.: Experimental Investigation of an Axial-Flow Supersonic Compressor Having Rounded Leading-Edge Blades With an 8-Percent Mean Thickness-Chord Ratio. NACA RM L53G16, 1953.

11. Huber, Paul W., and Kantrowitz, Arthur: A Device for Measuring Sonic Velocity and Compressor Mach Number. NACA TN 1664, 1948. (Supersedes NACA RM L6K14.)

12. Liepmann, Hans Wolfgang, and Puckett, Allen E.: Introduction to Aerodynamics of a Compressible Fluid. John Wiley & Sons, Inc., 1947.

13. Barnes, Norman F., and Bellinger, S. Lawrence: Schlieren and Shadowgraph Equipment for Air Flow Analysis. Jour. Optical Soc. of America, vol. 35, no. 8, Aug. 1945, pp. 497-509.

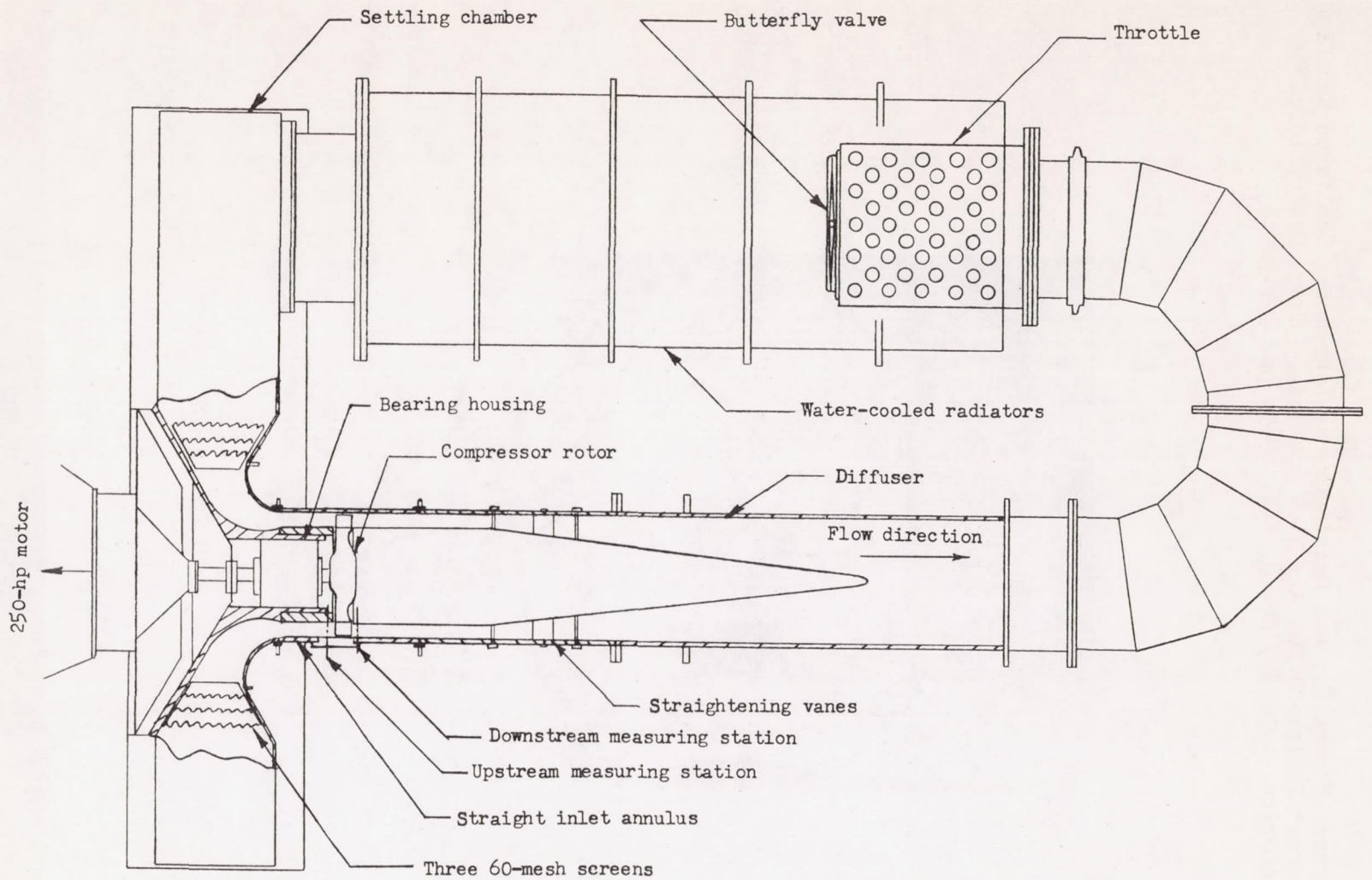

Figure 1.- Arrangement of the 250-horsepower compressor test stand.

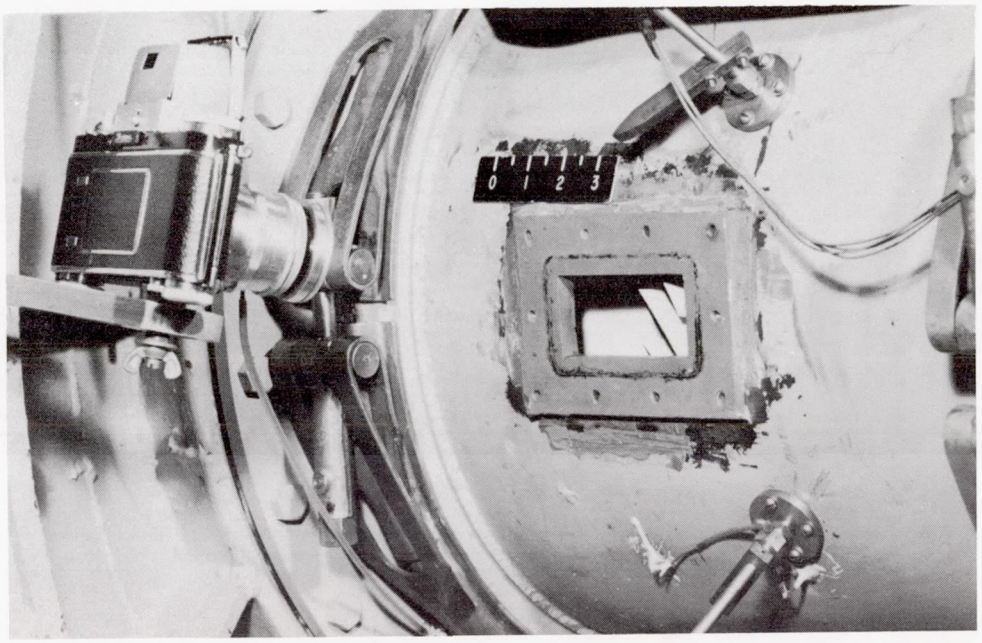

L-87785

Figure 2.- Camera location and observation window in outer casing of 250-horsepower test stand.

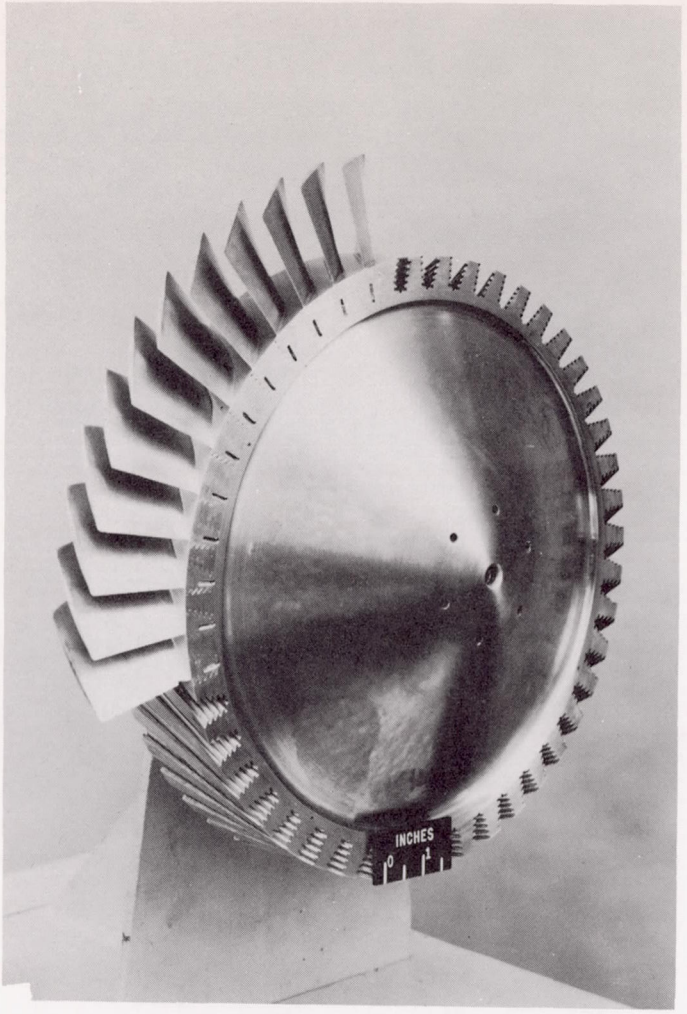

L-86020

(a) Sharp leading-edge rotor.

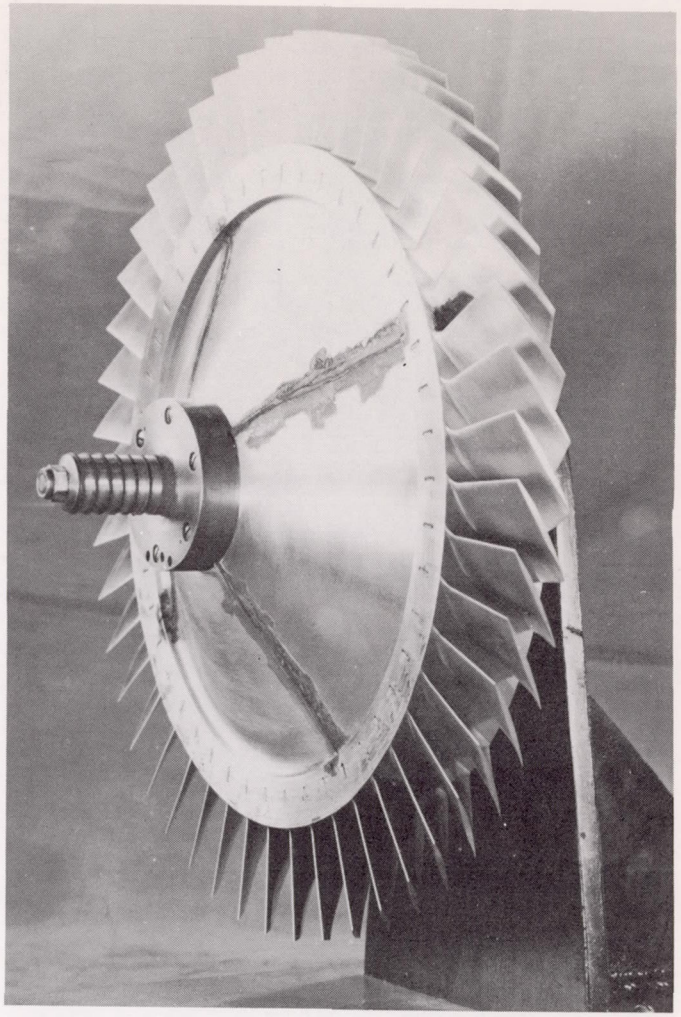

L-63386

(b) Rounded leading-edge rotor.

Figure 3.- Supersonic compressor test rotors.

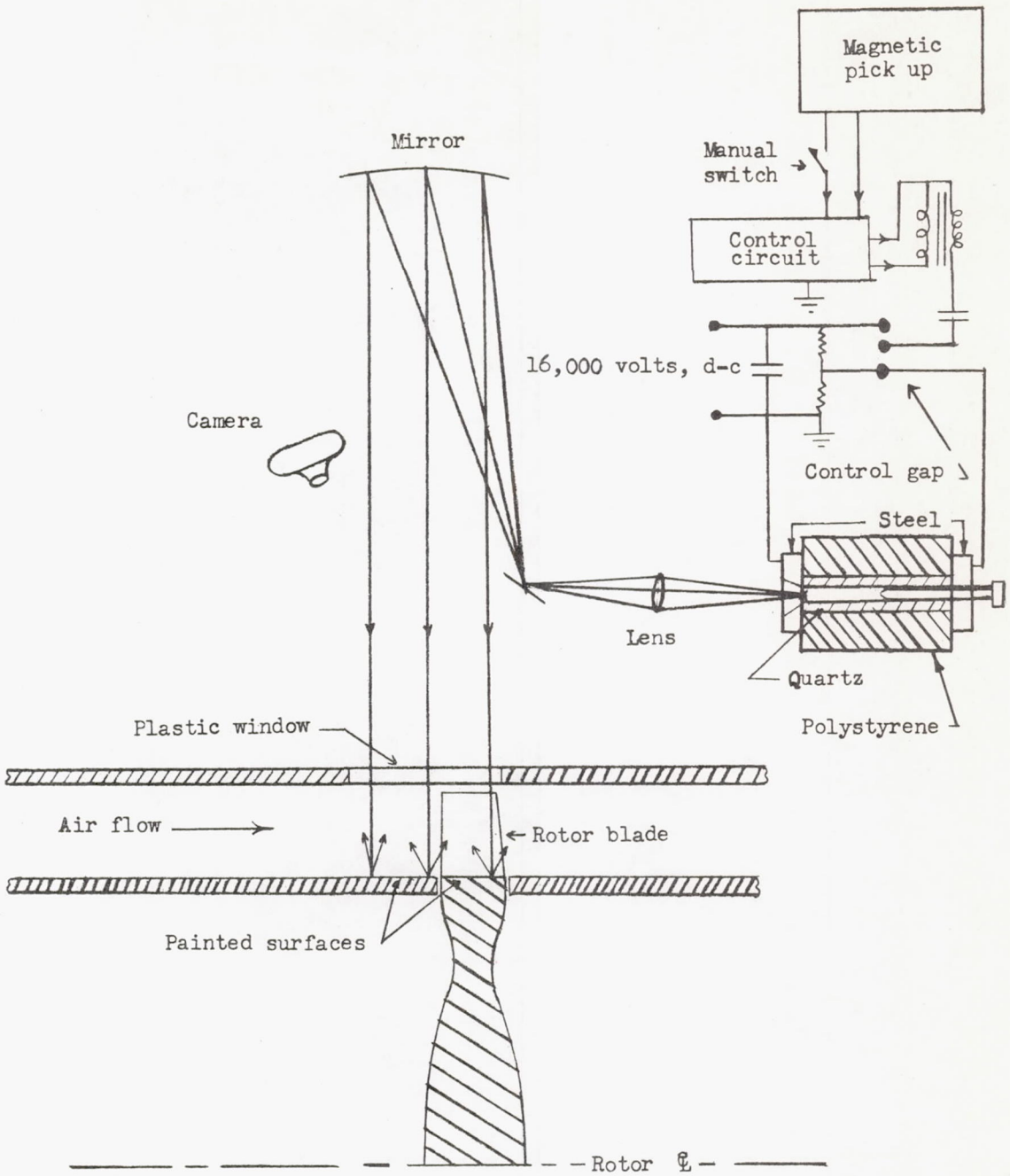

Figure 4.- Schematic diagram of shadowgraph apparatus.

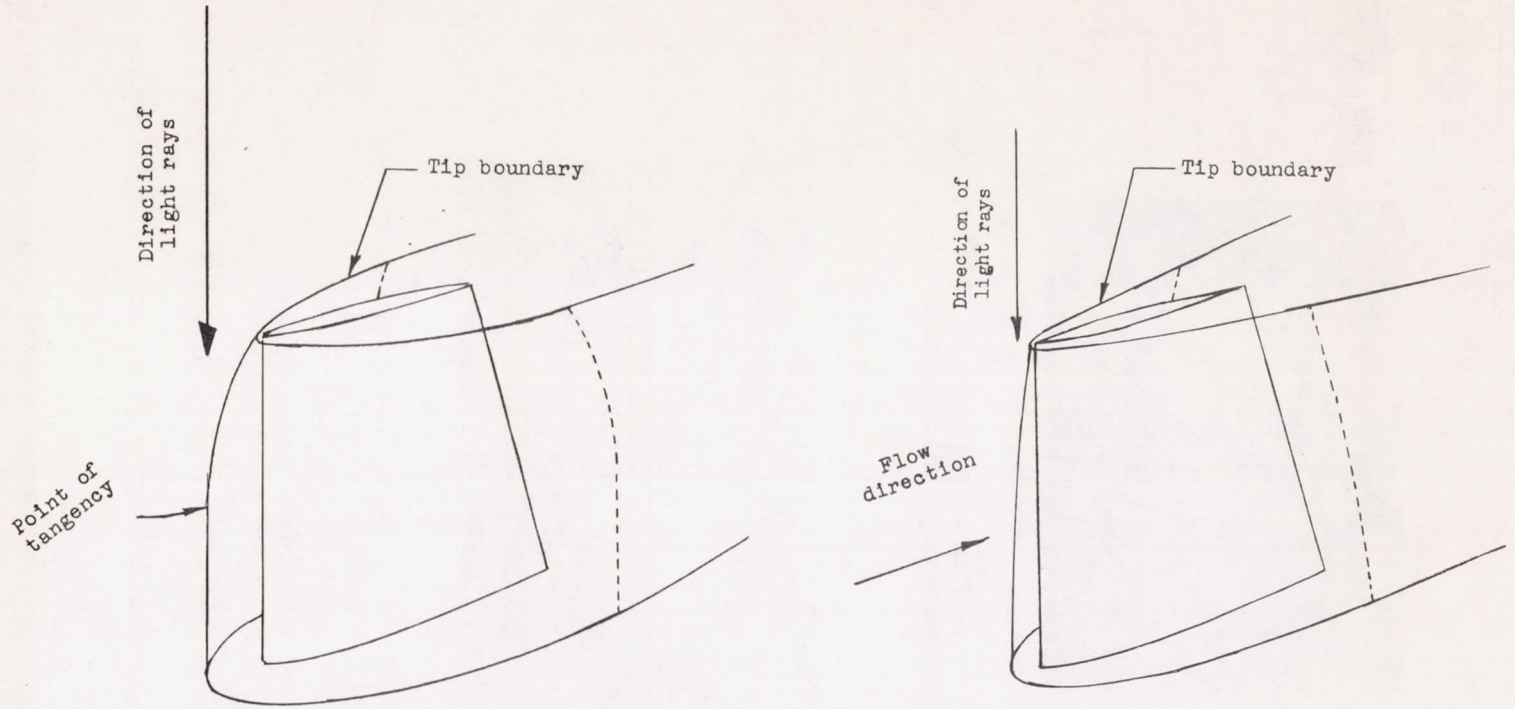

(a) Envelope from which two shocks would be expected; one from tip boundary and one from point of tangency.

(b) Envelope from which one shock would be expected; only from tip boundary.

Figure 5.- Probable types of shock envelopes.

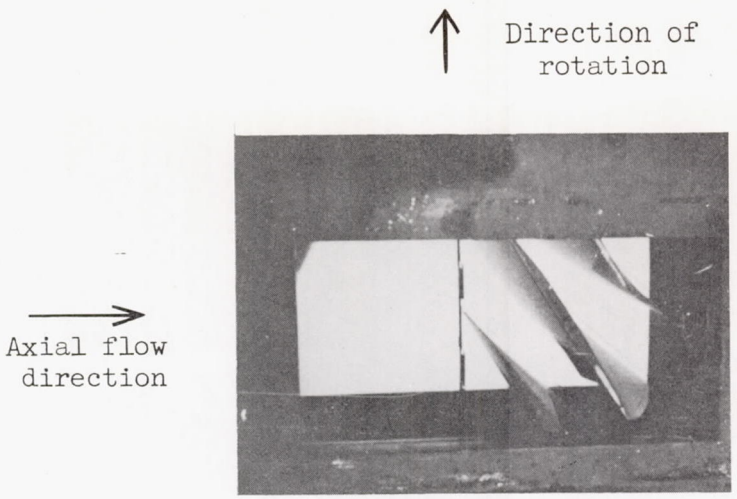

(a) Three-dimensional effect obtained by normal amount of illumination.

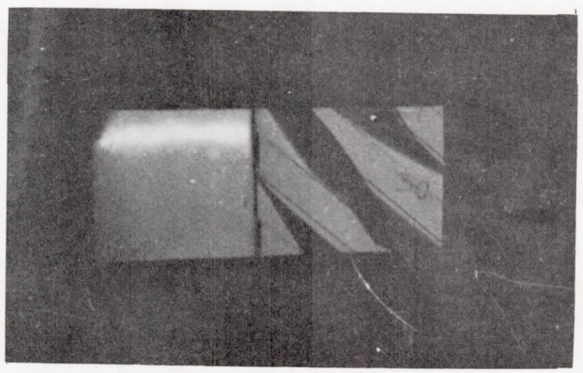

L-90681

(b) Blade silhouette obtained by illumination similar to that used for shadowgraphs.

Figure 6.- Photographs of stationary rotor through observation window.

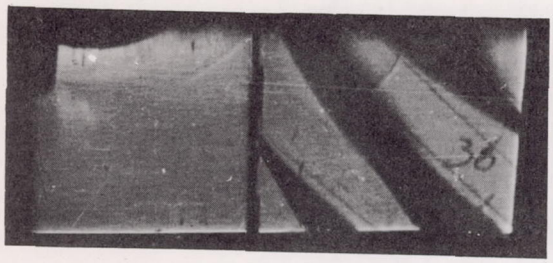

(a) $U_t/\sqrt{\theta}$ = 444 fps; P_2/P_1 = 1.14.

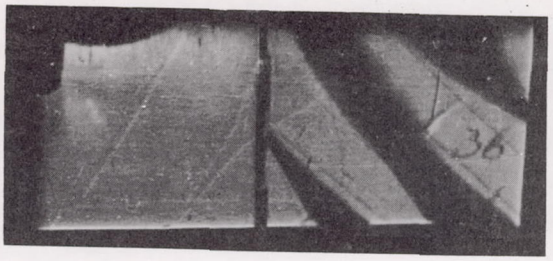

(d) $U_t/\sqrt{\theta}$ = 540 fps; P_2/P_1 = 1.20.

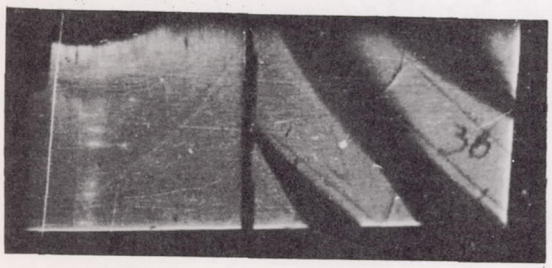

(b) $U_t/\sqrt{\theta}$ = 484 fps; P_2/P_1 = 1.16.

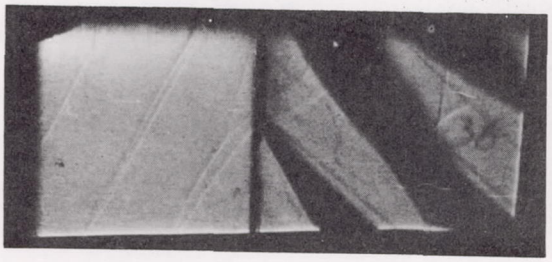

(e) $U_t/\sqrt{\theta}$ = 575 fps; P_2/P_1 = 1.22.

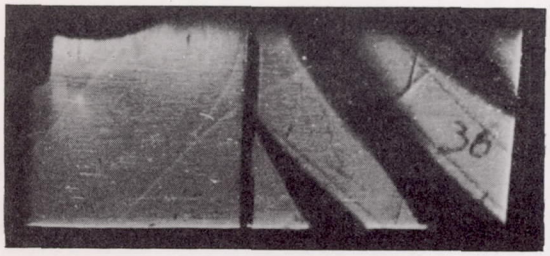

(c) $U_t/\sqrt{\theta}$ = 500 fps; P_2/P_1 = 1.18.

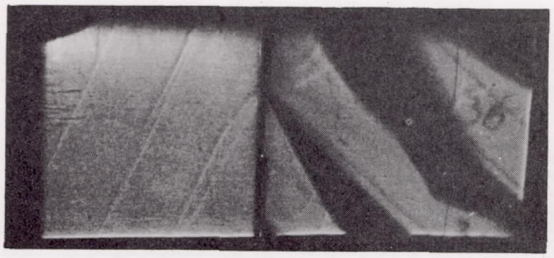

L-90686

(f) $U_t/\sqrt{\theta}$ = 610 fps; P_2/P_1 = 1.25.

Figure 7.- Shadowgraphs of sharp leading-edge rotor operating at near open throttle for varying speeds.

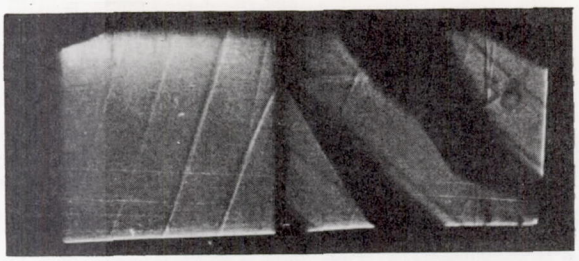

(g) $U_t/\sqrt{\theta}$ = 650 fps; P_2/P_1 = 1.26.

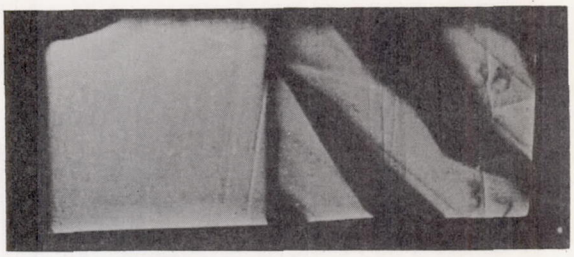

(j) $U_t/\sqrt{\theta}$ = 770 fps; P_2/P_1 = 1.31.

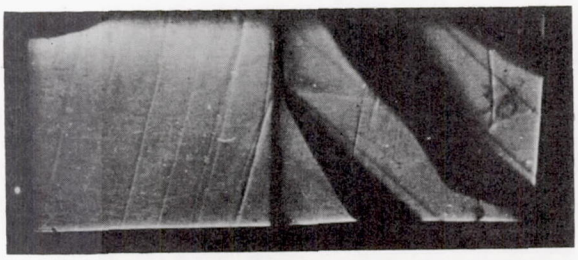

(h) $U_t/\sqrt{\theta}$ = 693 fps; P_2/P_1 = 1.27.

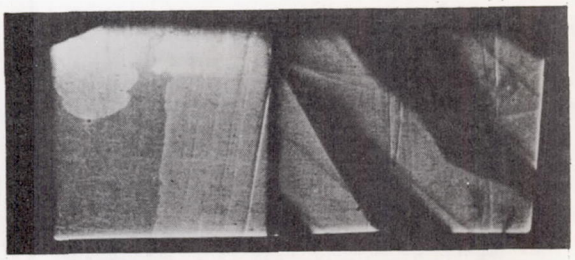

(k) $U_t/\sqrt{\theta}$ = 800 fps; P_2/P_1 = 1.31.

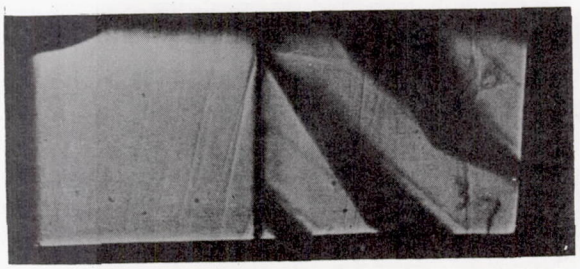

(i) $U_t/\sqrt{\theta}$ = 730 fps; P_2/P_1 = 1.30.

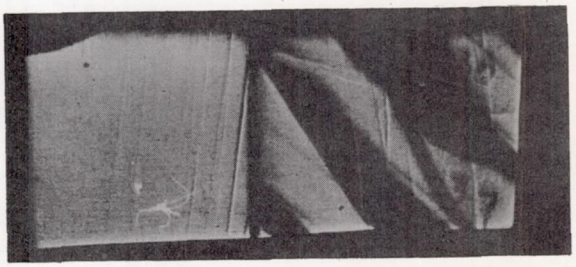

(l) $U_t/\sqrt{\theta}$ = 840 fps; P_2/P_1 = 1.32.

Figure 7.- Concluded. L-90689

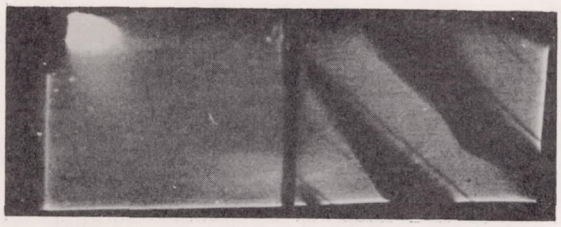

(a) $U_t/\sqrt{\theta}$ = 460 fps; P_2/P_1 = 1.15.

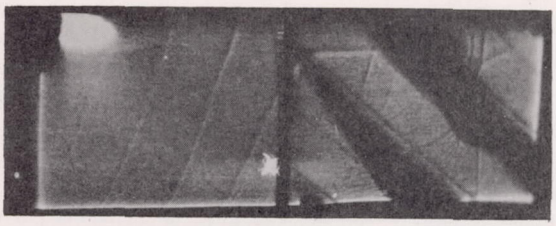

(f) $U_t/\sqrt{\theta}$ = 655 fps; P_2/P_1 = 1.24.

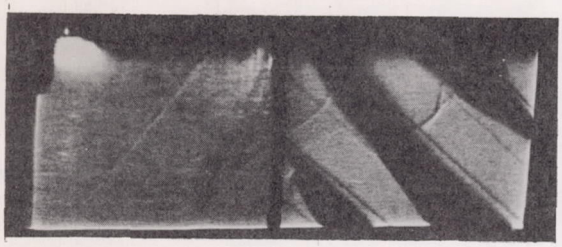

(b) $U_t/\sqrt{\theta}$ = 510 fps; P_2/P_1 = 1.20.

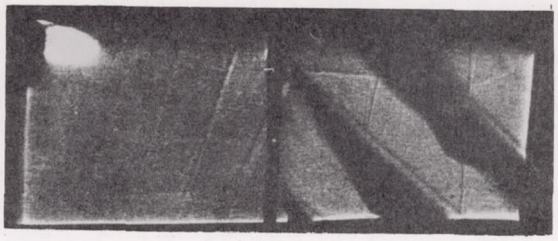

(g) $U_t/\sqrt{\theta}$ = 700 fps; P_2/P_1 = 1.26.

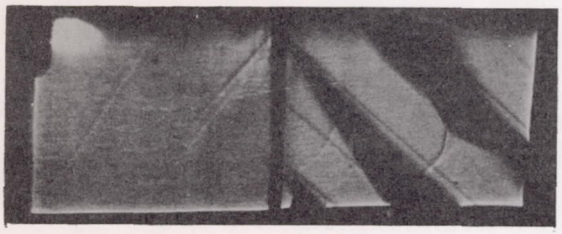

(c) $U_t/\sqrt{\theta}$ = 545 fps; P_2/P_1 = 1.23.

(h) $U_t/\sqrt{\theta}$ = 740 fps; P_2/P_1 = 1.36.

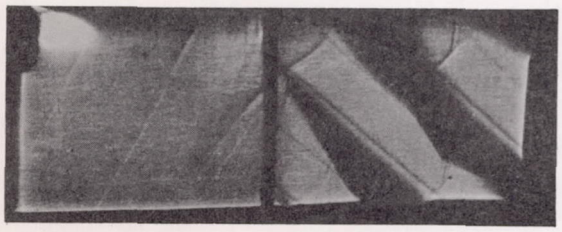

(d) $U_t/\sqrt{\theta}$ = 580 fps; P_2/P_1 = 1.23.

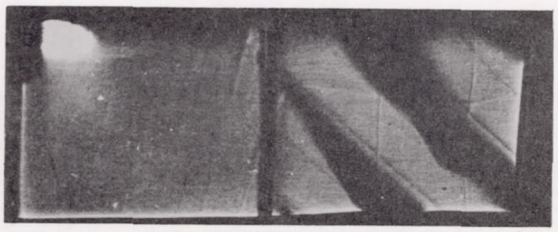

(i) $U_t/\sqrt{\theta}$ = 775 fps; P_2/P_1 = 1.32.

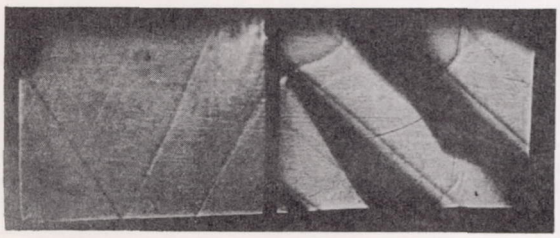

(e) $U_t/\sqrt{\theta}$ = 620 fps; P_2/P_1 = 1.29.

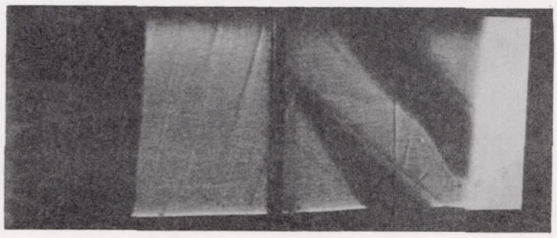

(j) $U_t/\sqrt{\theta}$ = 820 fps; P_2/P_1 = 1.35.

Figure 8.- Shadowgraphs of rounded leading-edge rotor operating at near open throttle for varying speeds.

L-90682

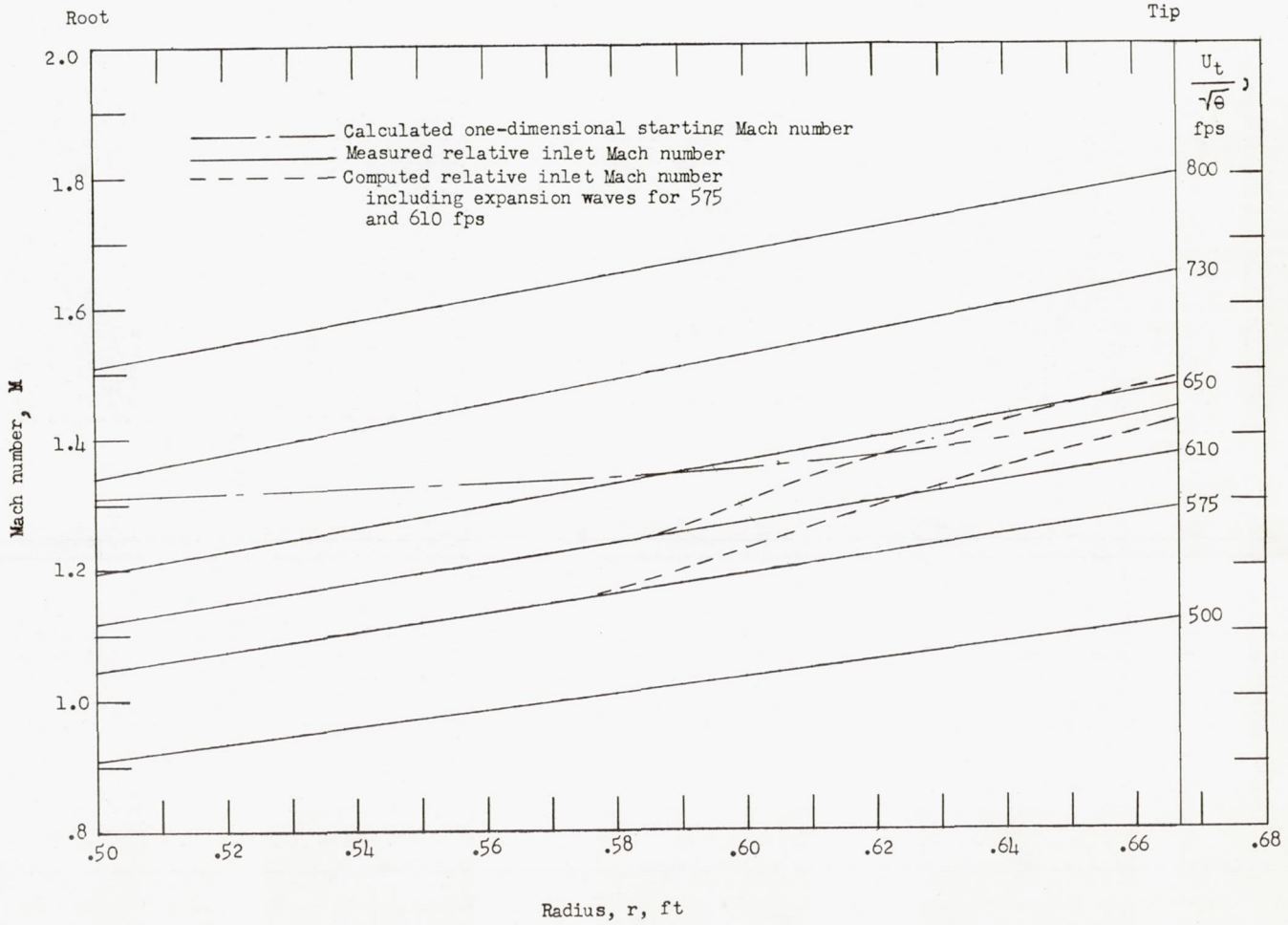

Figure 9.- Variation of starting Mach number and relative inlet Mach number as a function of radius over range of equivalent tip speeds for sharp leading-edge rotor.

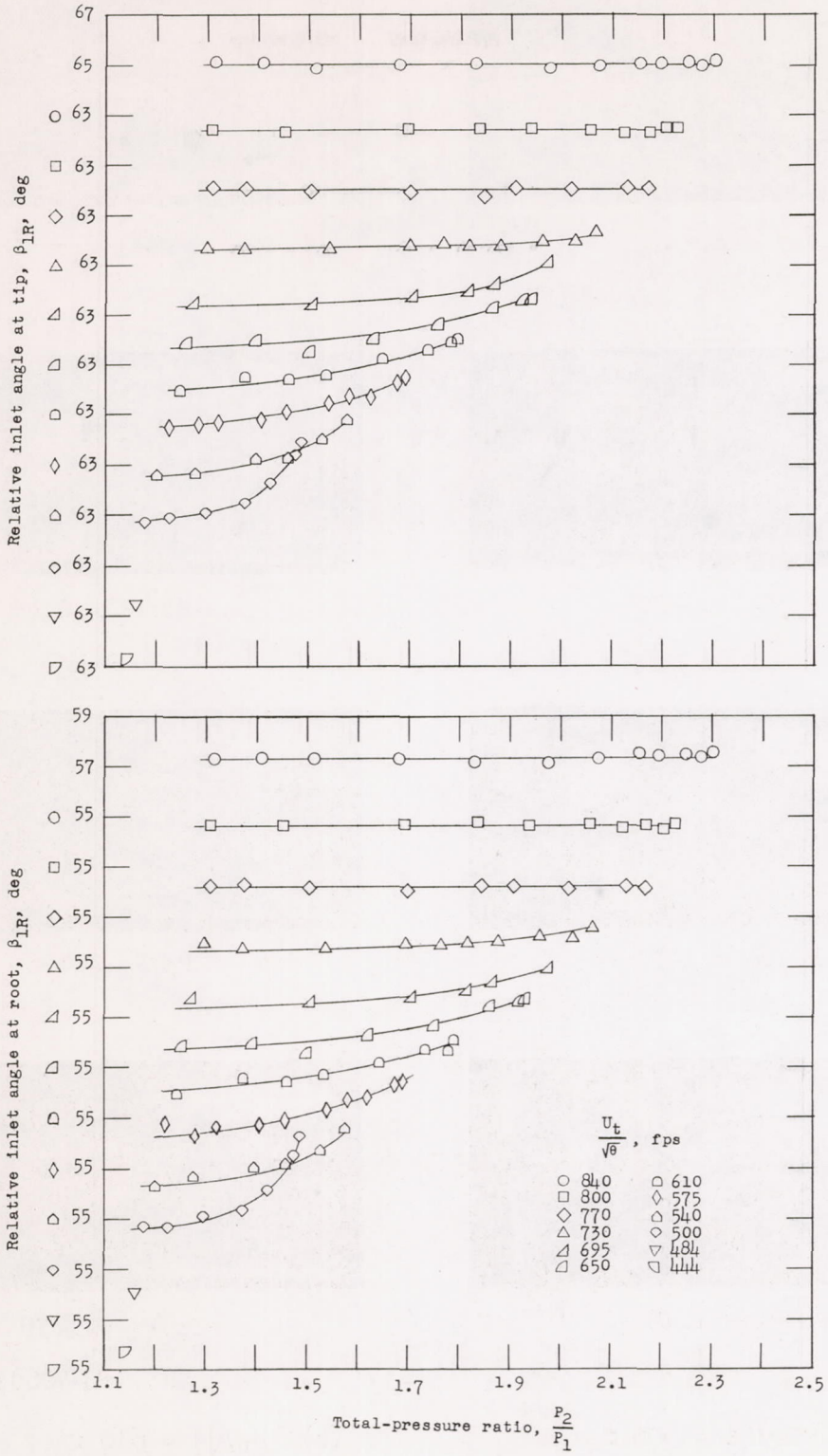

Figure 10.- Variation of relative inlet angle at tip and root with total-pressure ratio for sharp leading-edge rotor.

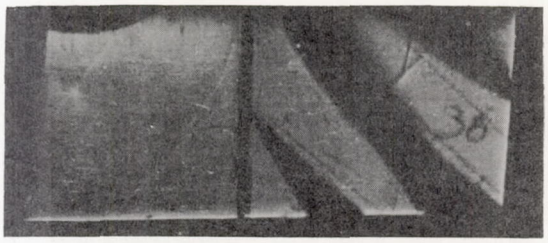

P_2/P_1 = 1.18

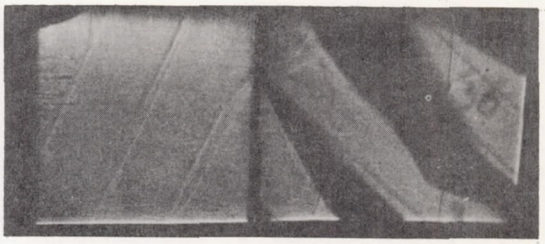

P_2/P_1 = 1.25

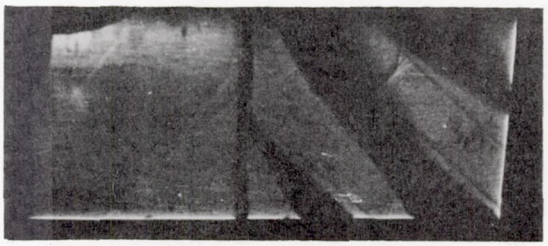

P_2/P_1 = 1.22

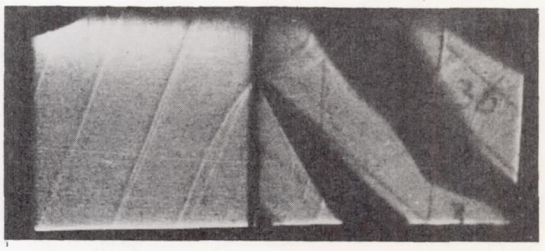

P_2/P_1 = 1.46

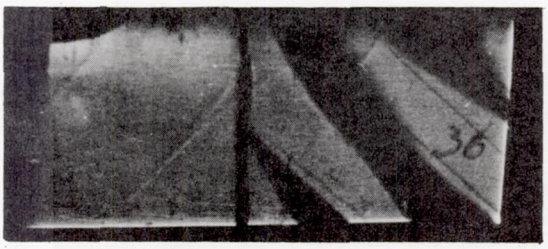

P_2/P_1 = 1.37

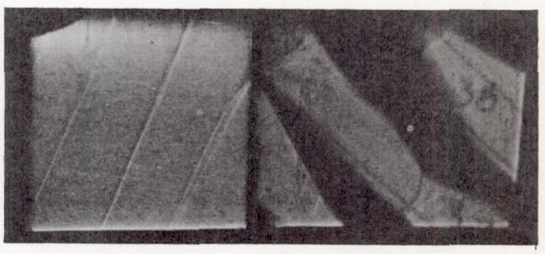

P_2/P_1 = 1.60

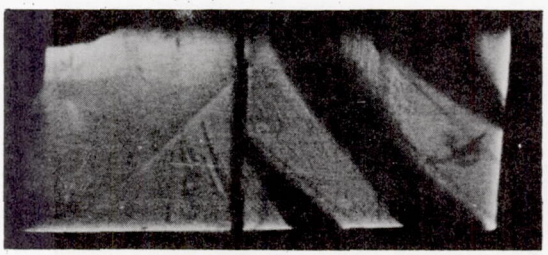

P_2/P_1 = 1.49

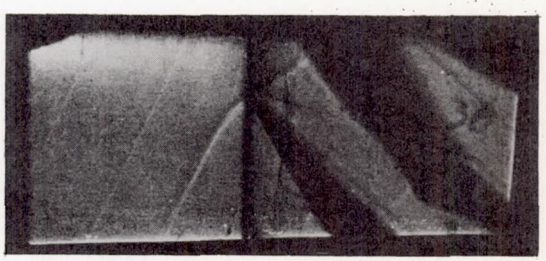

P_2/P_1 = 1.78

L-90683

(a) $U_t/\sqrt{\theta}$ = 500 fps. (b) $U_t/\sqrt{\theta}$ = 610 fps.

Figure 11.- Shadowgraphs of sharp leading-edge rotor operating at various speeds with varying throttle settings.

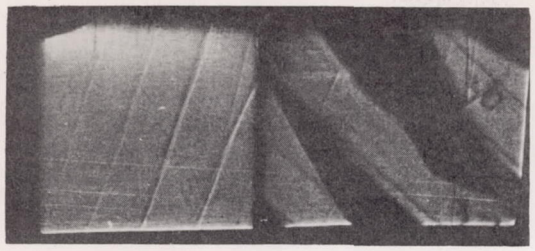

P_2/P_1 = 1.26

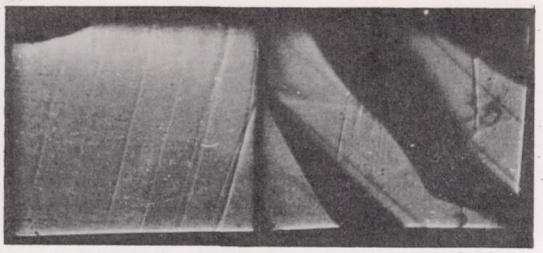

P_2/P_1 = 1.27

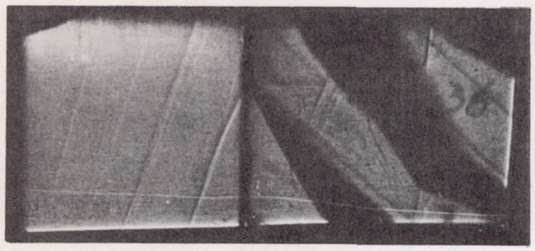

P_2/P_1 = 1.63

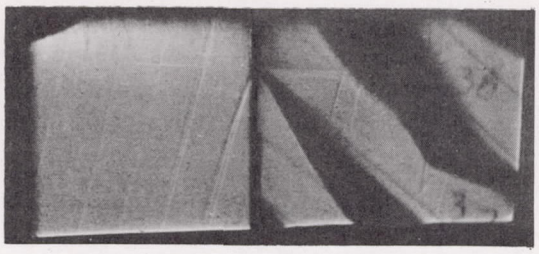

P_2/P_1 = 1.62

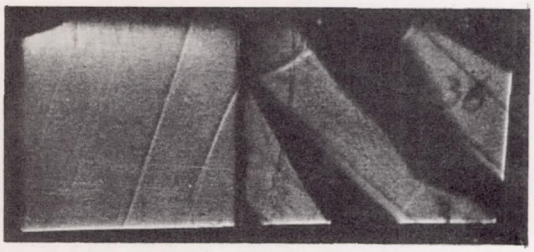

P_2/P_1 = 1.75

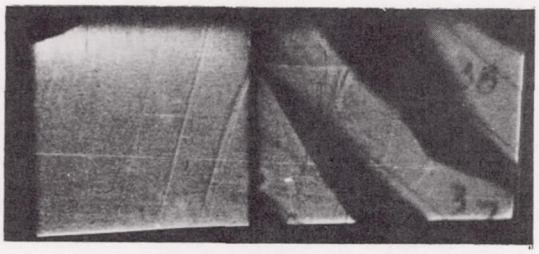

P_2/P_1 = 1.87

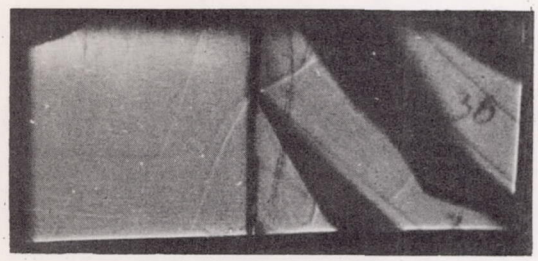

P_2/P_1 = 1.92

(c) $U_t/\sqrt{\theta}$ = 650 fps.

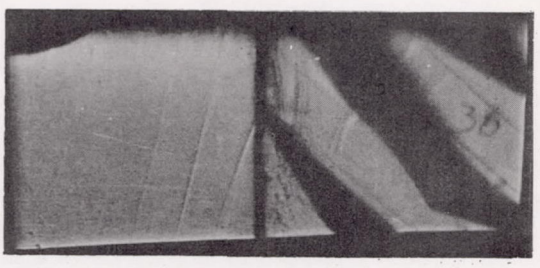

P_2/P_1 = 1.97

(d) $U_t/\sqrt{\theta}$ = 695 fps.

L-90687

Figure 11.- Continued.

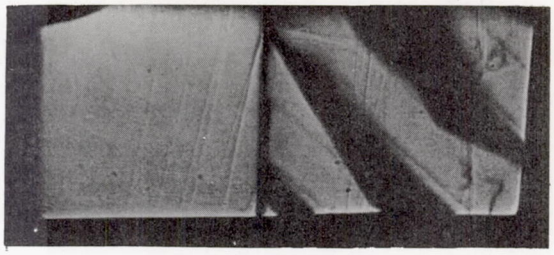

P_2/P_1 = 1.30

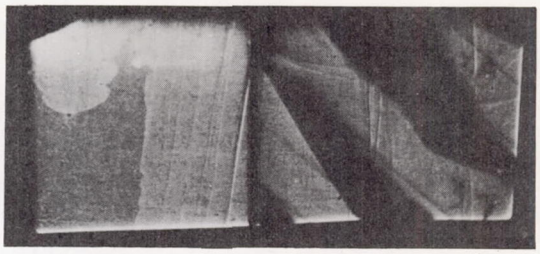

P_2/P_1 = 1.31

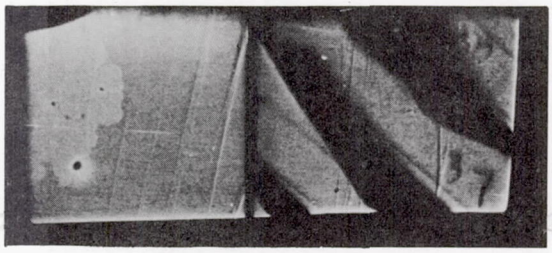

P_2/P_1 = 1.45

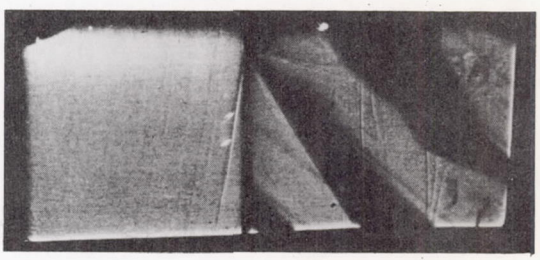

P_2/P_1 = 1.59

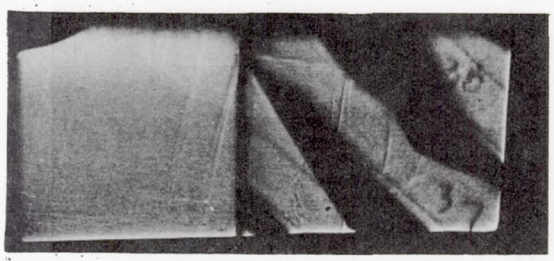

P_2/P_1 = 1.77

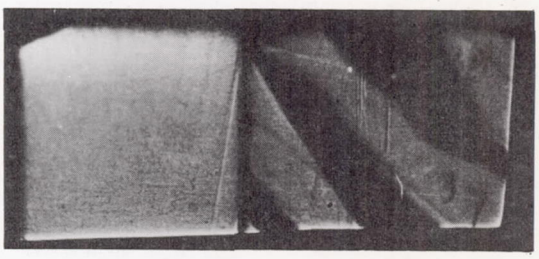

P_2/P_1 = 1.98

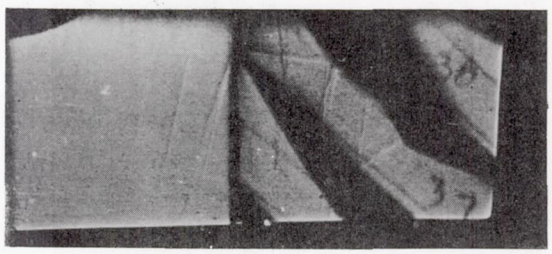

P_2/P_1 = 2.00

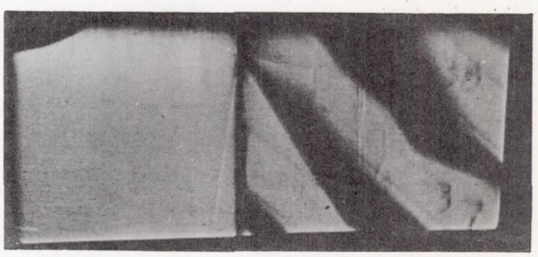

P_2/P_1 = 2.21

(e) $U_t/\sqrt{\theta}$ = 730 fps.

(f) $U_t/\sqrt{\theta}$ = 800 fps.

Figure 11.- Concluded.

L-90685

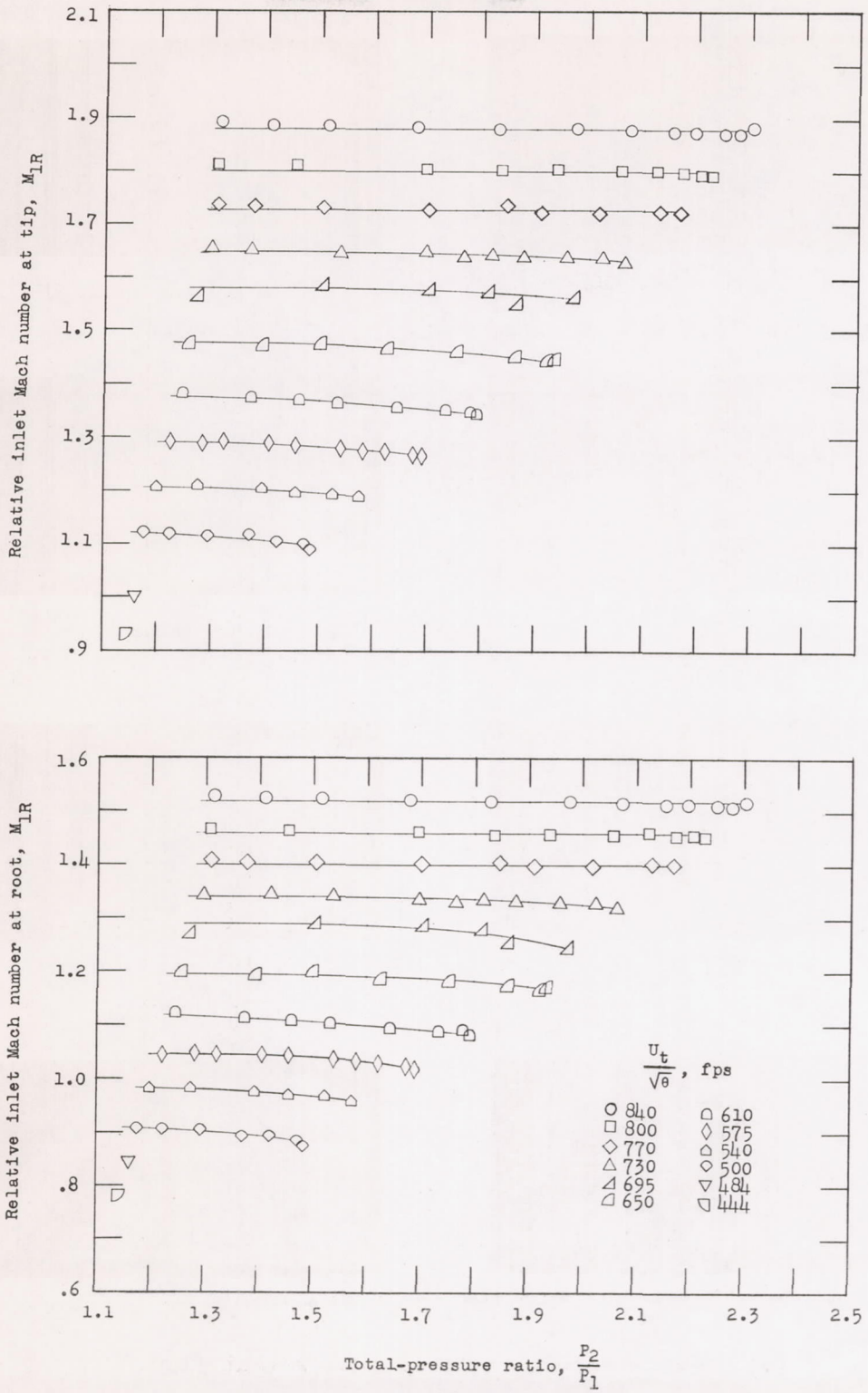

Figure 12.- Variation of relative inlet Mach number at tip and root with total-pressure ratio for sharp leading-edge rotor.

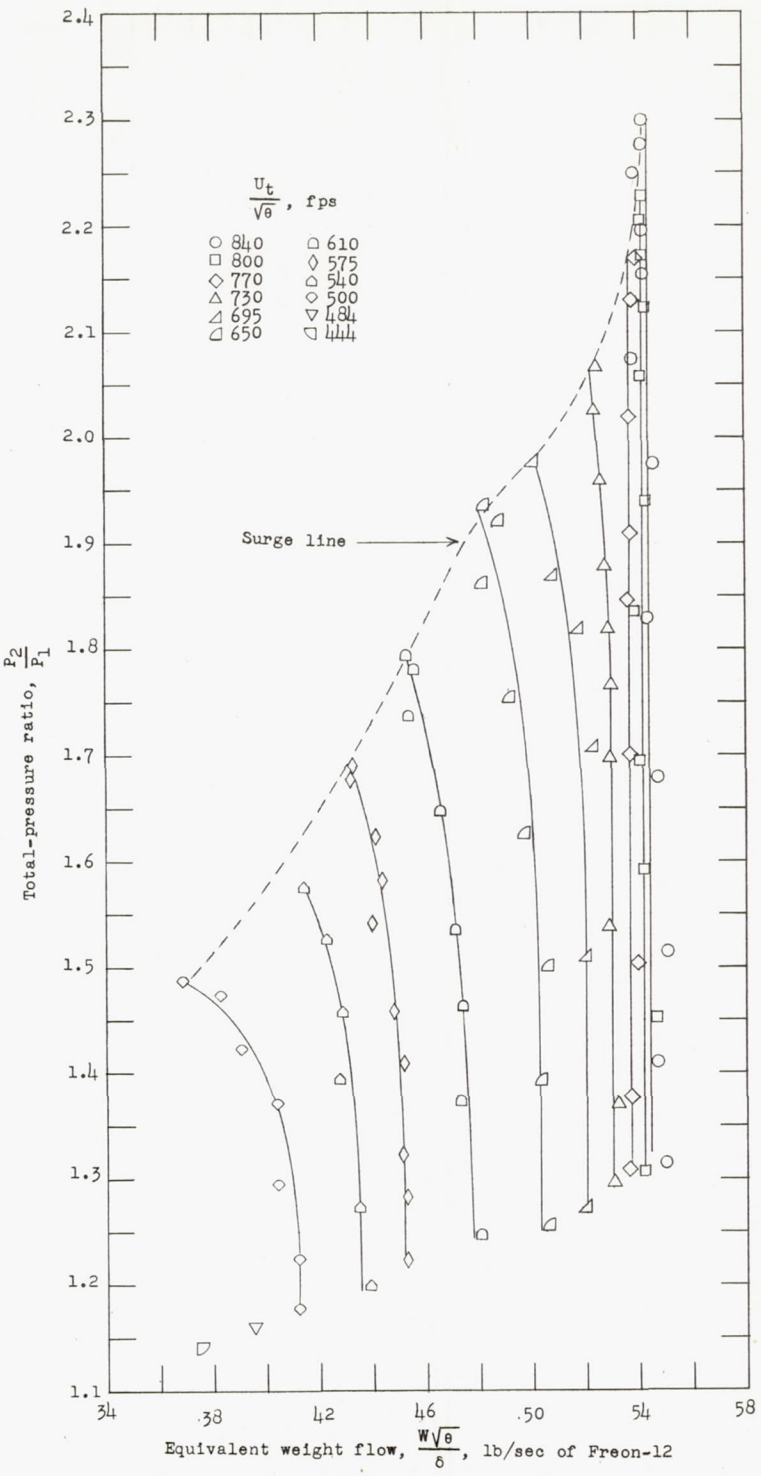

(a) Total-pressure ratio against weight flow.

Figure 13.- Performance characteristics of sharp leading-edge rotor without guide vanes. Results obtained in Freon-12.

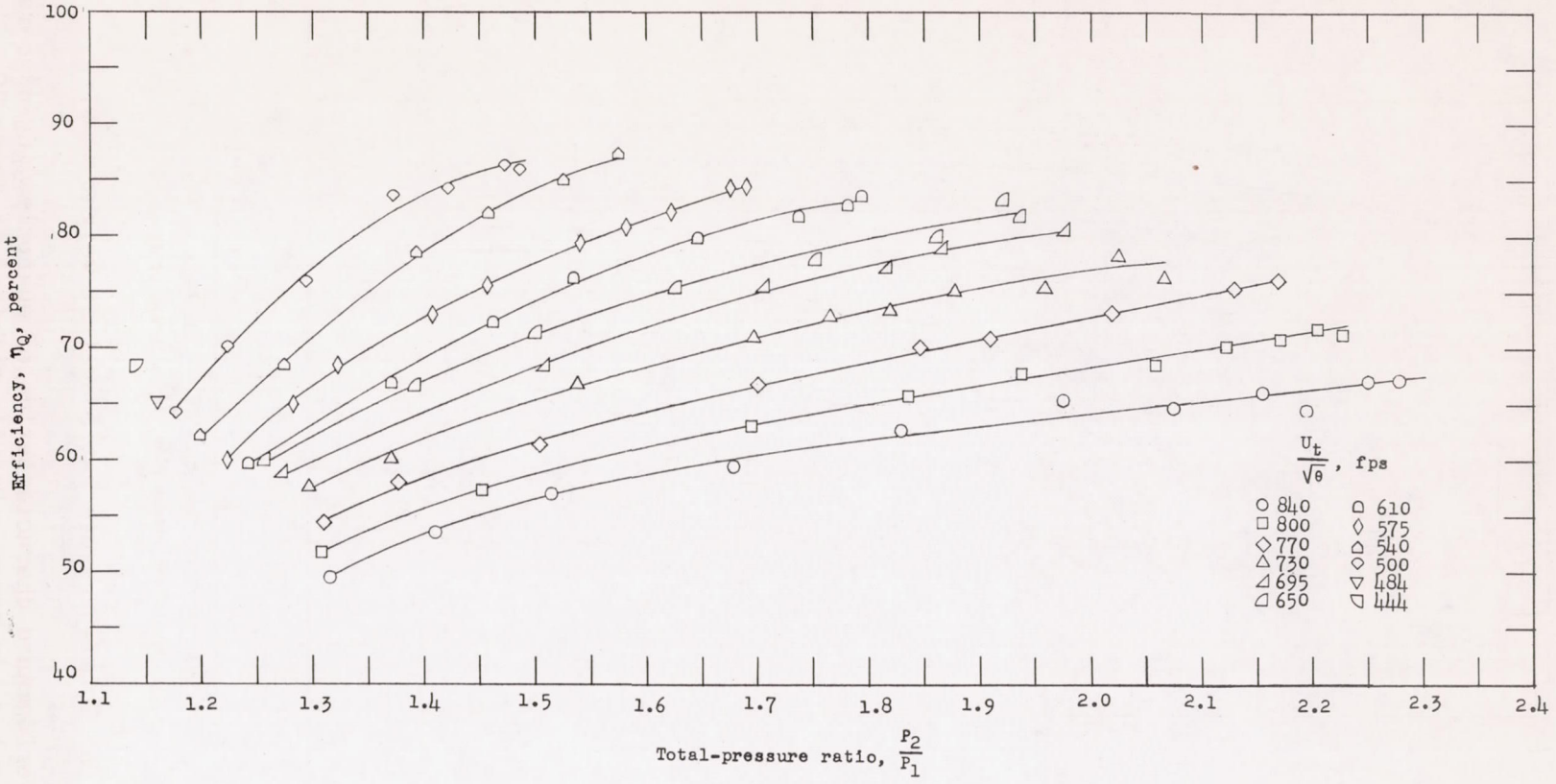

(b) Total pressure ratio against efficiency.

Figure 13.- Concluded.

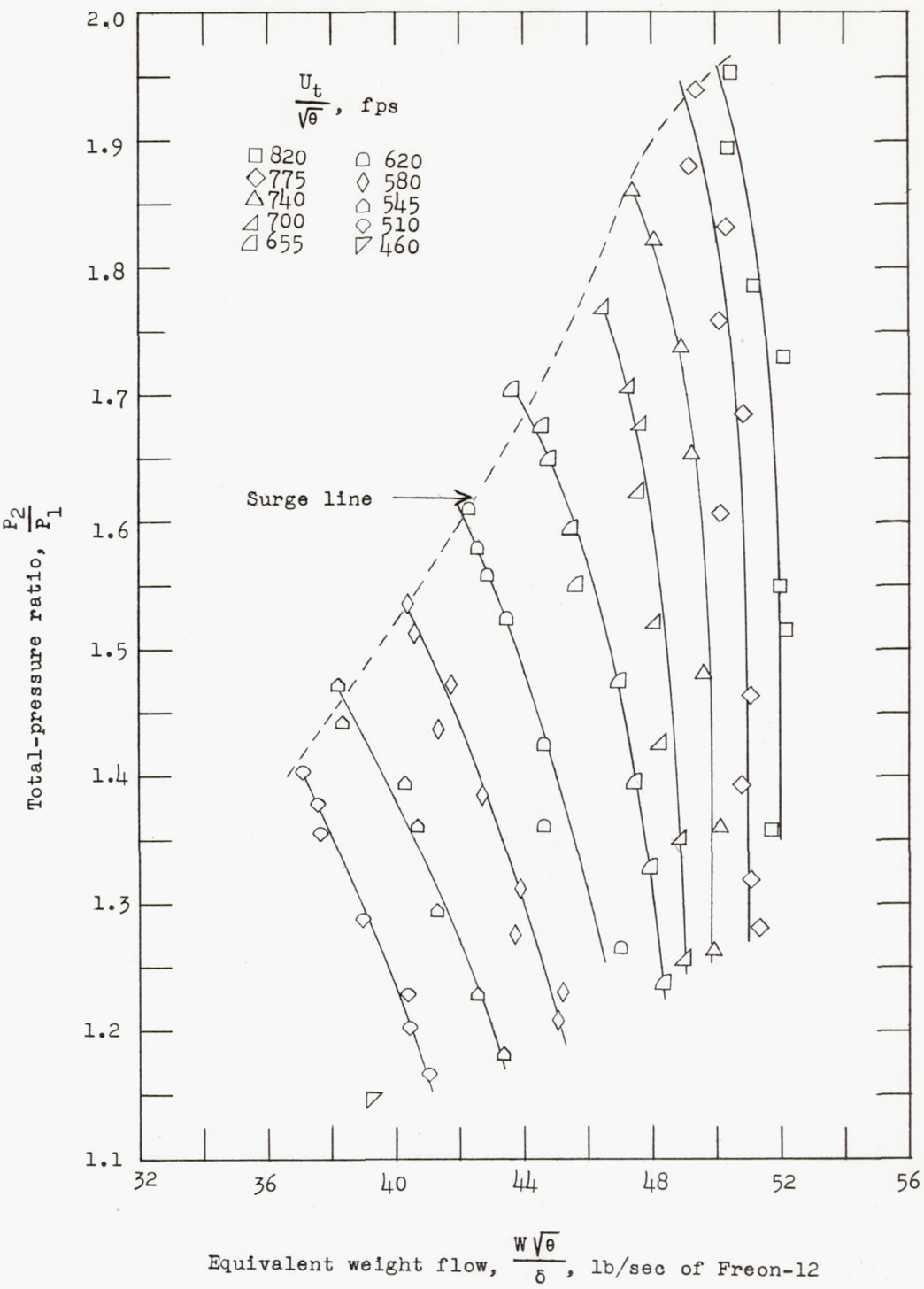

(a) Total-pressure ratio against weight flow.

Figure 14.- Performance characteristics of rounded leading-edge rotor without guide vanes. Results obtained in Freon-12.

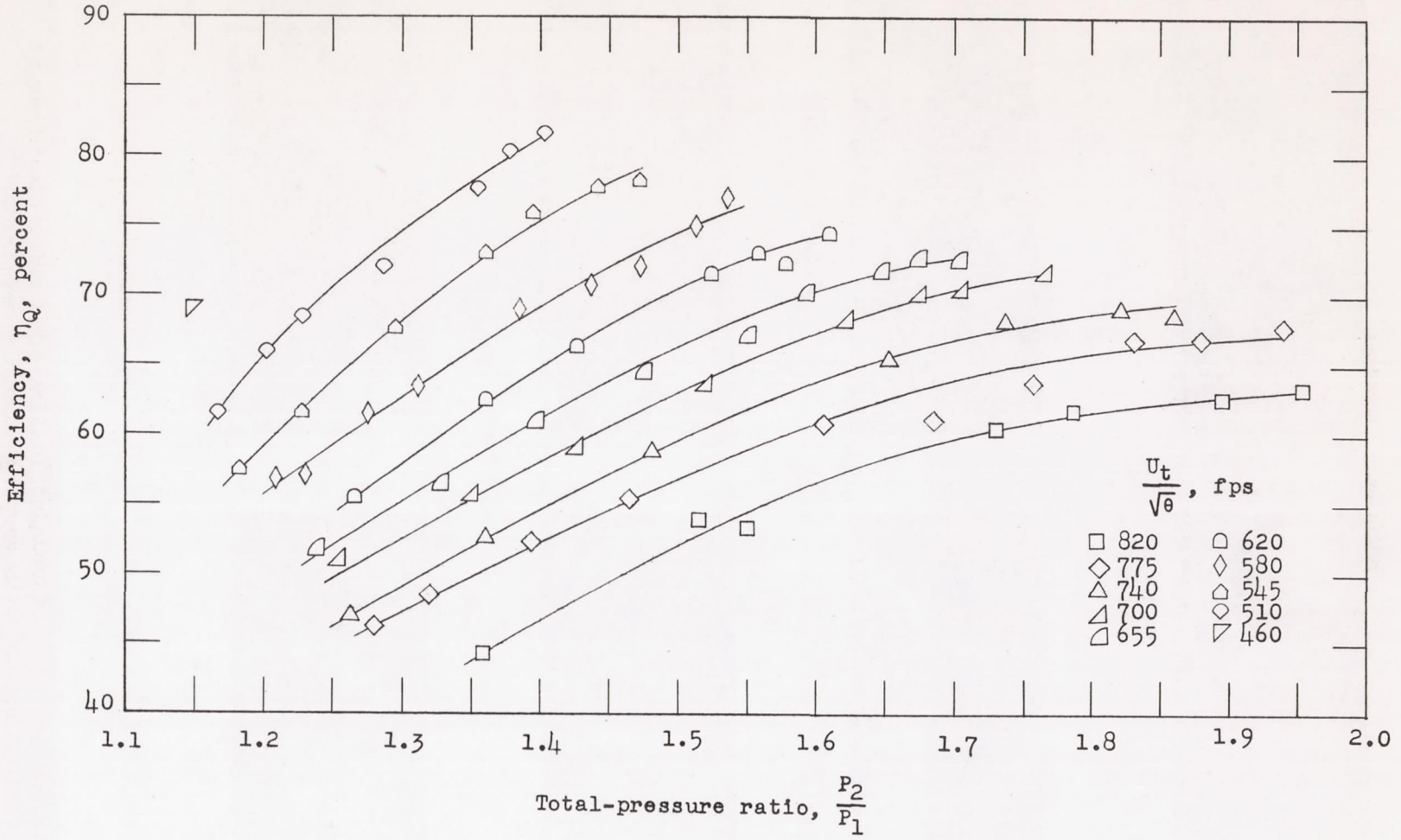

(b) Total-pressure ratio against efficiency.

Figure 14.- Concluded.

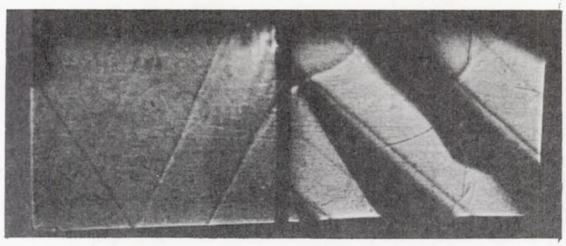

P_2/P_1 = 1.29

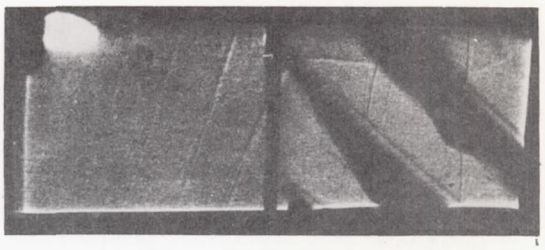

P_2/P_1 = 1.26

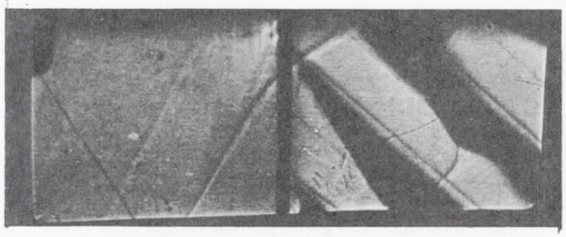

P_2/P_1 = 1.39

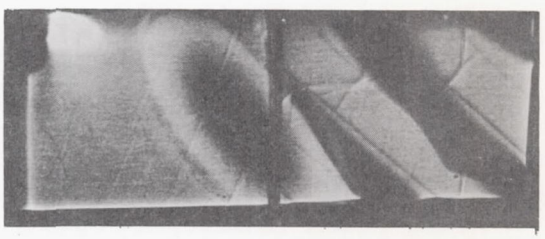

P_2/P_1 = 1.39

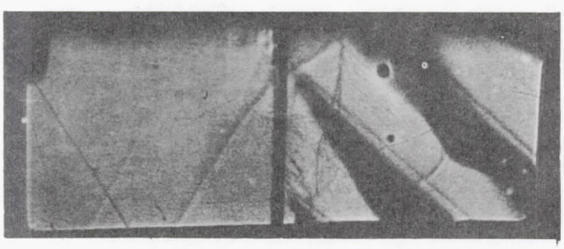

P_2/P_1 = 1.52

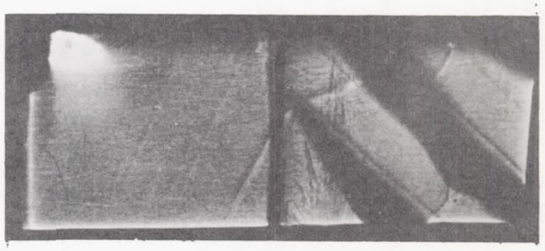

P_2/P_1 = 1.59

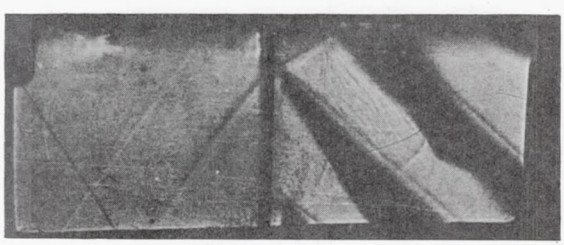

P_2/P_1 = 1.60

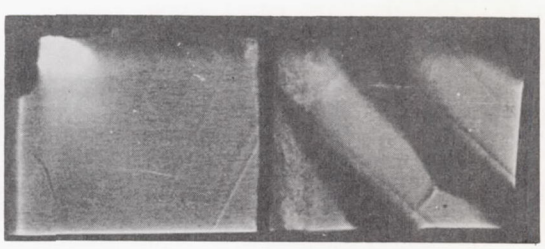

P_2/P_1 = 1.74

(a) $U_t/\sqrt{\theta}$ = 620 fps.

(b) $U_t/\sqrt{\theta}$ = 700 fps.

L-90684

Figure 15.- Shadowgraphs of rounded leading-edge rotor operating at various speeds with varying throttle settings.

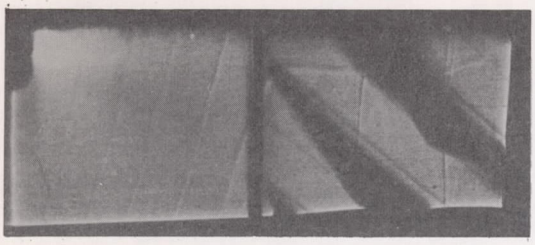

P_2/P_1 = 1.36

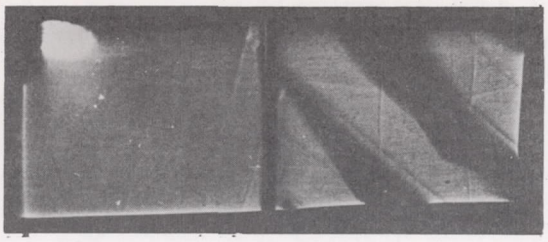

P_2/P_1 = 1.32

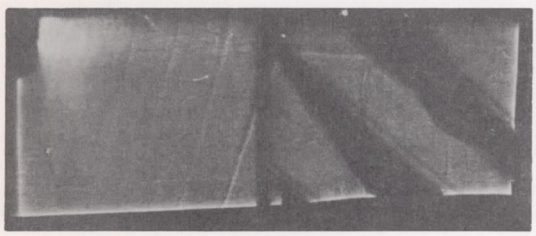

P_2/P_1 = 1.48

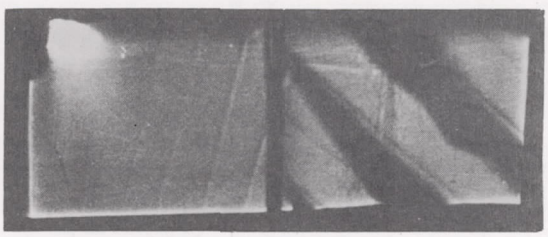

P_2/P_1 = 1.46

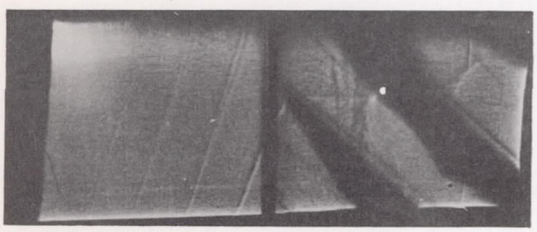

P_2/P_1 = 1.74

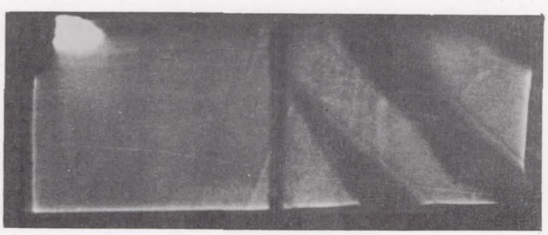

P_2/P_1 = 1.64

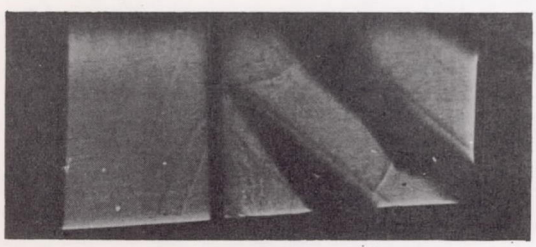

P_2/P_1 = 1.86

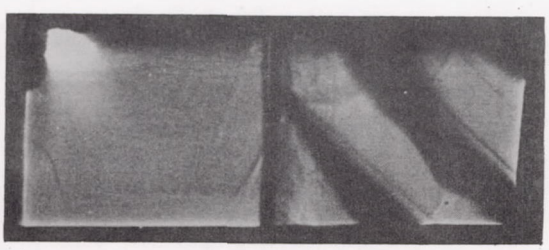

P_2/P_1 = 1.88

(c) $U_t/\sqrt{\theta}$ = 740 fps.

(d) $U_t/\sqrt{\theta}$ = 775 fps.

Figure 15.- Concluded.

L-90688

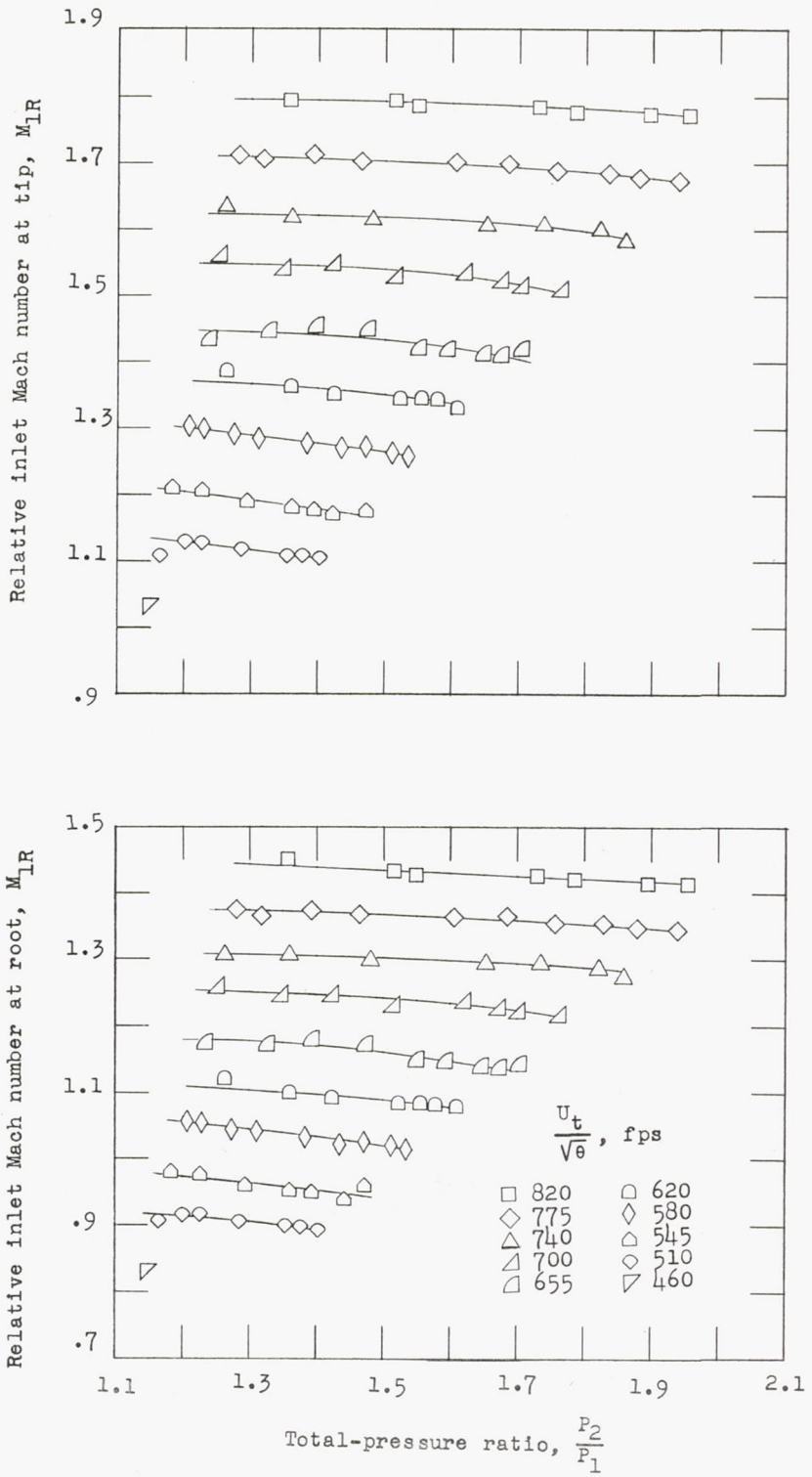

Figure 16.- Variation of relative inlet Mach number at tip and root with total-pressure ratio for rounded leading-edge rotor.

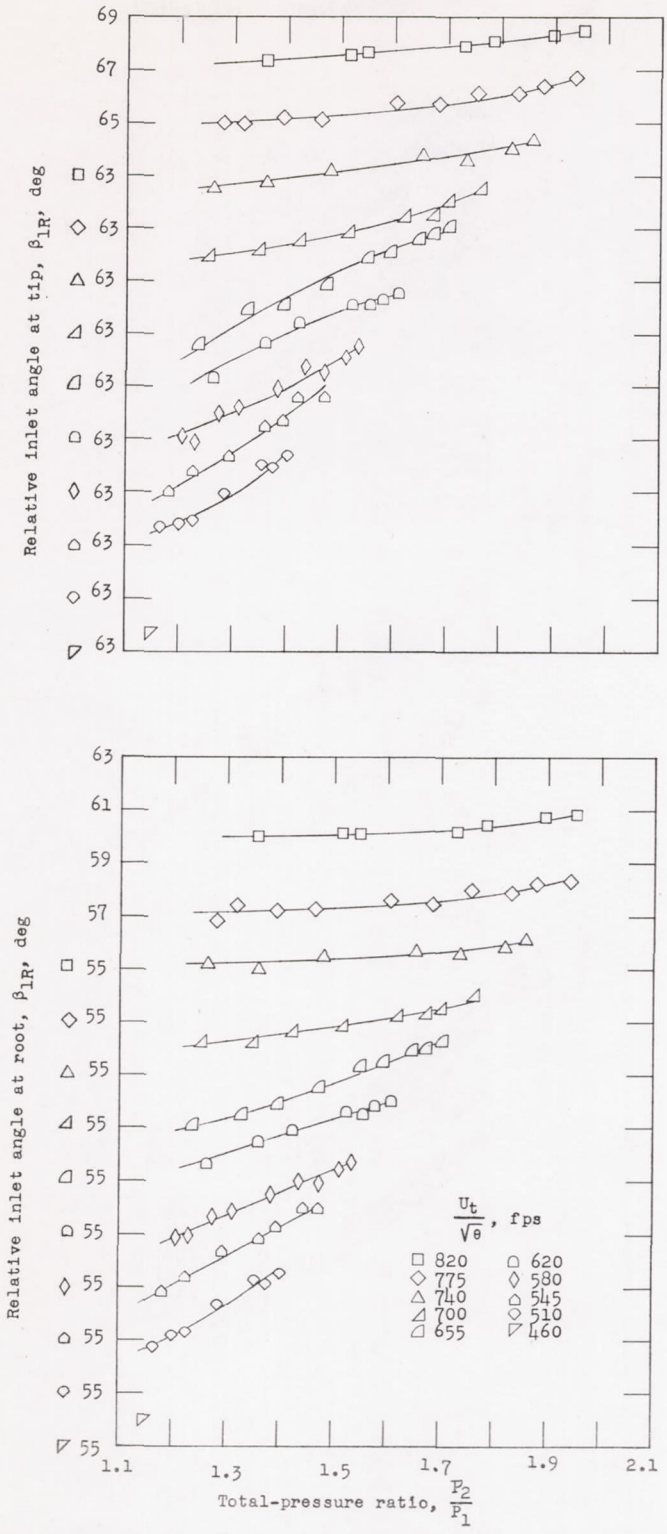

Figure 17.- Variation of relative inlet angle at tip and root with total pressure for rounded leading-edge rotor.

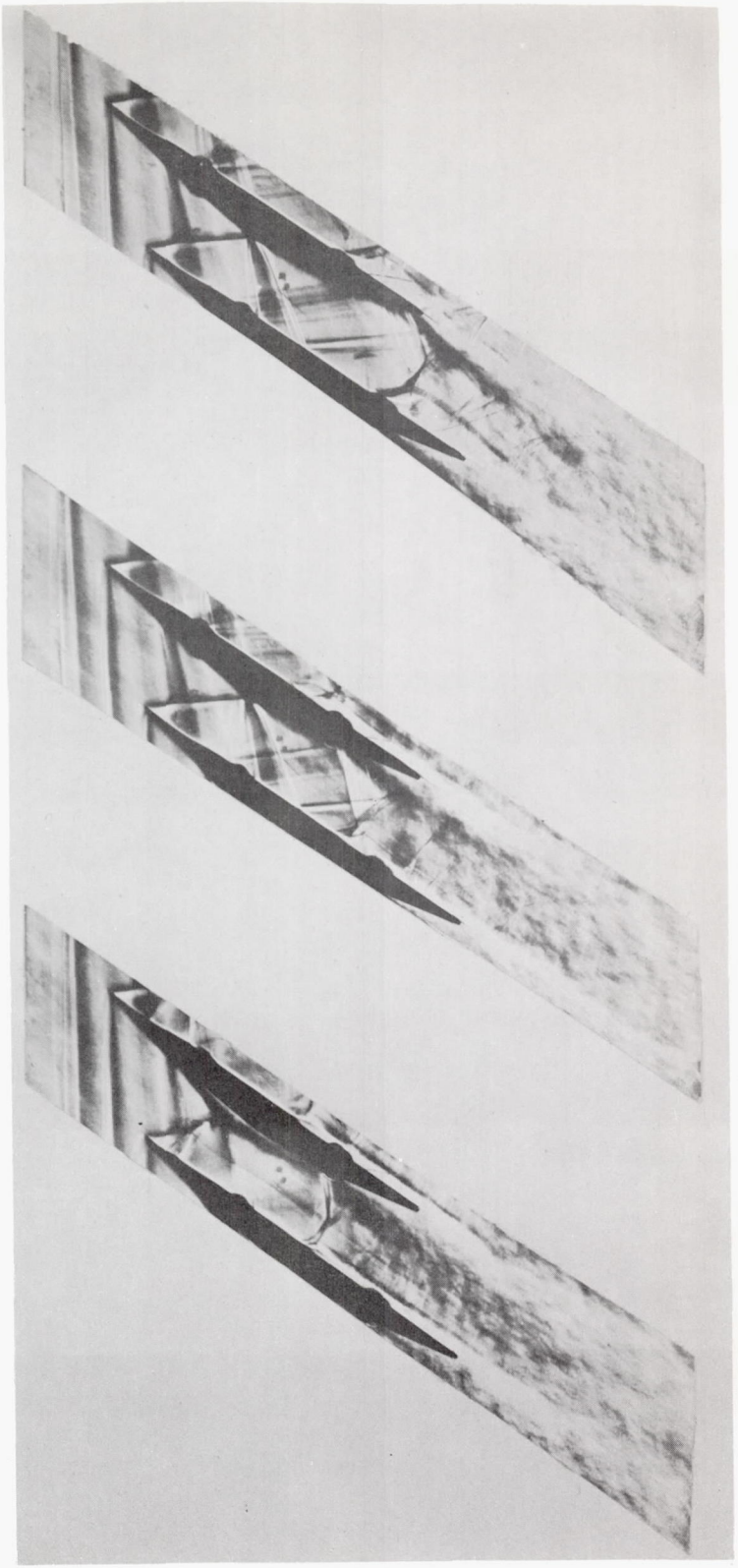

L-90680

Figure 18.- Schlieren photographs of pitch section in two-dimensional cascade.

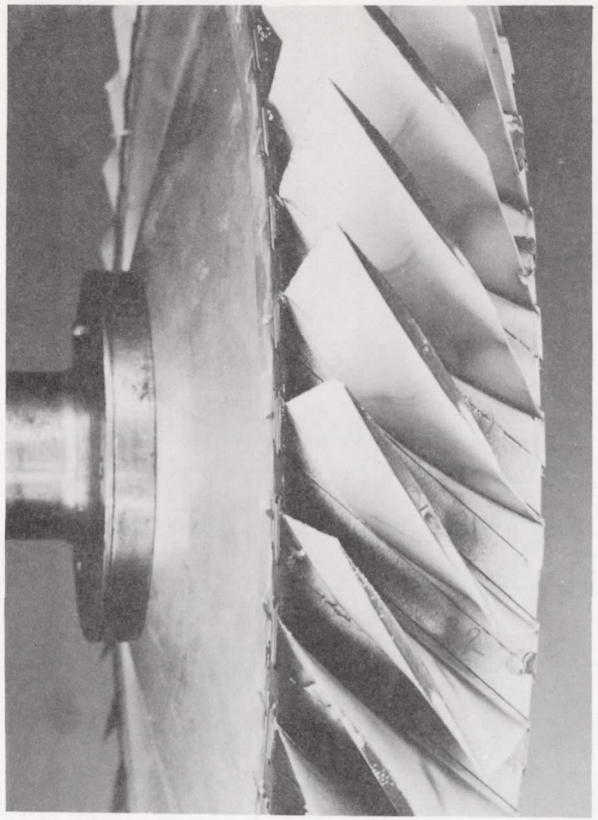

(a) Rotor.

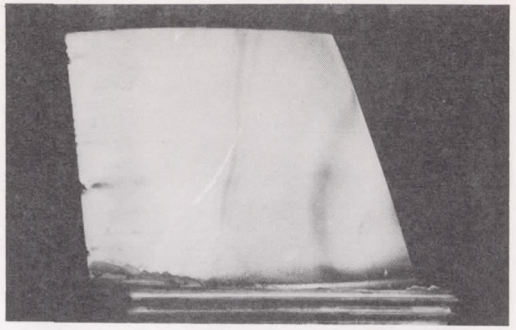

(b) Suction surface of blade.

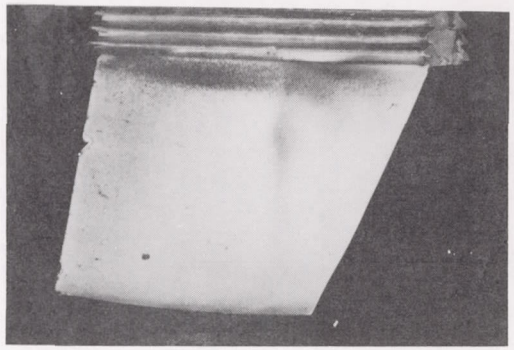

(c) Pressure surface of blade.

L-91711

Figure 19.- Dust patterns obtained with sharp leading-edge rotor showing location of shocks.

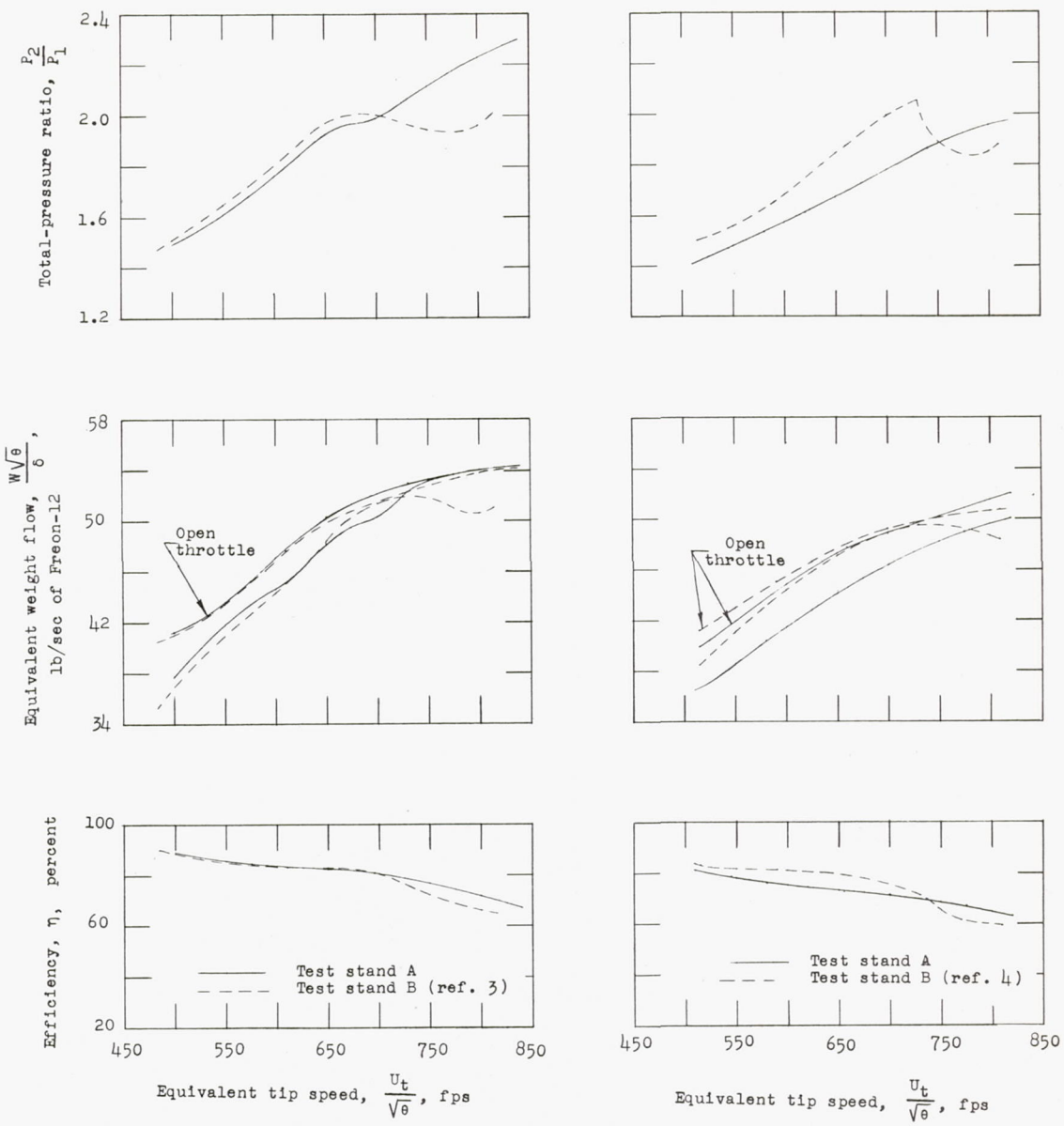

(a) Sharp leading-edge rotor. (b) Rounded leading-edge rotor.

Figure 20.- Comparison of results obtained in different compressor test stands. All curves are for maximum throttle condition unless otherwise noted.